Bantidi and Nishimura
Earth, Planets and Space (2022) 74:117
https://doi.org/10.1186/s40623-022-01677-4

Earth, Planets and Space

FULL PAPER

Spatio-temporal clustering of successive earthquakes as inferred from analyses of global CMT and NIED F-net catalogs

Thystere Matondo Bantidi* and Takeshi Nishimura

Abstract

Investigation of the characteristic behavior of successive earthquakes that closely occur in space and time is important to understand the generation mechanism of earthquakes and useful to assess a triggered earthquake, especially around the area, where a first large earthquake took place. Here, we analyzed the Global Centroid Moment Tensor catalog from 1976 to 2016 for shallow earthquakes with a moment magnitude, M_W, of at least 5.5, and the F-net catalog, Japan, for $4 \leq M_W < 5.5$, to clarify the spatio-temporal characteristics of the successive earthquakes. We first sorted all of the earthquakes in time and removed the aftershocks that occurred in and around the faults of earthquakes with M_W larger than the target magnitude range we investigated. Then, we selected source events from the beginning and searched for earthquakes that occurred within a horizontal distance (D) and a lapsed time (T_a) from the source event to group them in clusters. Then, the source event was selected from the catalog in order, and the same procedure was repeated. We counted the number of clusters, each of which consisted of successive earthquakes, for different D and T_a. To examine whether successive earthquakes were explained by random occurrences, we compared the results with simulations in which earthquakes occurred randomly in time but at the same locations matching the centroids in the real data. The comparison showed that the number of clusters for the simulation rapidly increased with D and merged with that for real data at a short distance, which is defined here as the triggering distance. We find that triggering distance is proportional to about 1/5 to 1/4 of the seismic moment (M_0) of the source event, and exponentially decreases with increasing T_a. Relating the derived empirical scaling relations between M_0 and triggering distance from the equations in the ETAS model, we show that the observed exponents of 1/5 to 1/4 were well predicted from the estimated ETAS parameters in various regions around the world. These consistencies first show that successive occurrence of earthquakes is well explained by the ETAS model.

Keywords: Spatio-temporal clustering, Successive earthquake occurrence, Triggering distance, Coulomb stress change, ETAS model, Tectonic setting

*Correspondence: tbantidi@gmail.com

Department of Geophysics, Graduate School of Science, Tohoku University, 6-3 Aramaki-aza Aoba, Aoba-ku, Sendai 980-8578, Japan

Graphical abstract

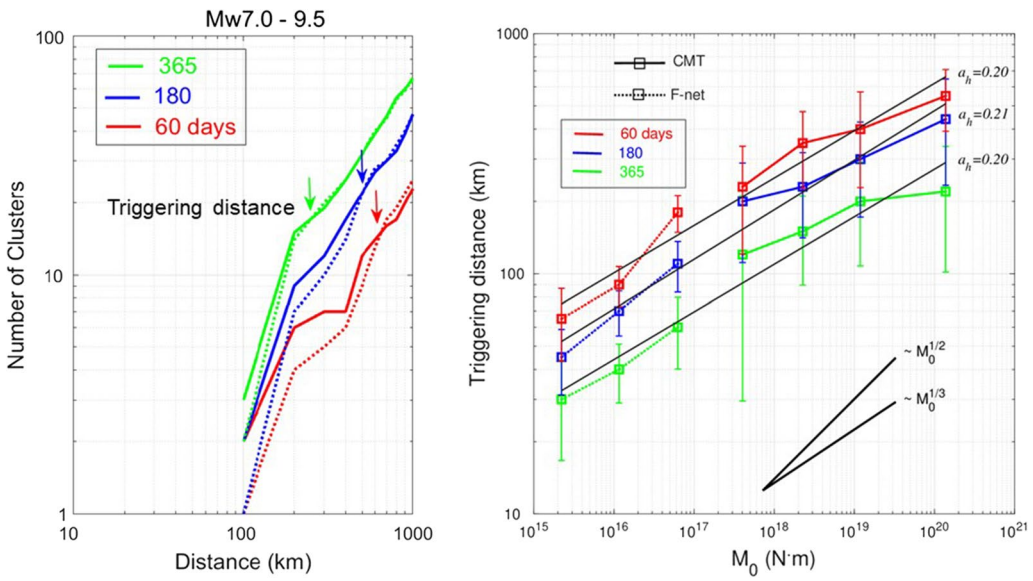

Introduction

Seismic activity is often characterized by a sequence of earthquakes that is based on the largest earthquake, which is called the mainshock. The mainshock, which is sometimes preceded by foreshocks, is often followed by aftershocks (Omori 1894; Dascher-Cousineau et al. 2020). Another way to characterize seismic activity is to group it into two types (Hicks 2011; Zaliapin and Ben-Zion 2016): One consists of independent events that are related to slower deformation processes due to visco-elastic behavior in the crust and mantle, and/or the ambient stress field due to, for example, plate tectonic motion. The earthquakes categorized this way may form background seismicity, which is generally explained by a homogeneous process or stationary Poisson process (Hicks 2011; Zaliapin and Ben-Zion 2016). The other type consists of dependent events that are entirely or partially triggered by previous events (e.g., mainshocks) (Hicks 2011; Zaliapin and Ben-Zion 2016). Several methods have been proposed to distinguish independent seismicity (background seismicity) and dependent seismicity (triggered seismicity), which are often referred to as earthquake clustering and declustering (van Stiphout et al. 2012).

The earthquake occurrence process (i.e., seismicity) is often treated as a point process in space and time with a magnitude M (Daley and Vere-Jones 2003; de Arcangelis et al. 2008), and is often described by some universal empirical relations. One of the most important empirical laws for seismicity is the Gutenberg–Richter law, which states that the occurrence frequency of earthquakes versus magnitudes M is expressed by the equation $\log N = a - bM$, where N is the number of earthquakes with a magnitude of at least M, and a and b are constants (Gutenberg and Richter 1944). Another one is the modified Omori law, which states that the occurrence rate for earthquakes after a large earthquake (i.e., mainshock) decays in proportion to t^{-p}, where t is the time from the mainshock and p a constant (Utsu 2002). These two empirical laws have been used for evaluating the seismic activity and/or seismic hazard after a large earthquake occurs. For example, Parsons (2002) analyzed earthquakes occurring after large earthquakes with magnitudes of $M_s \geq 7.0$ using the Global Centroid Moment Tensor (CMT) catalog for the period from 1977 to 2000, and found that the aftershocks continue for 7–11 years after the main shock, obeying the modified Omori law. He further indicated that shear stress in the aftershock area increases up to 240 km away from the centroid of the mainshock. Recently, the Epidemic Type Aftershock Sequence (ETAS) model has been widely used (Ogata 1988, 1998). The ETAS model has evolved from the formulations by Ogata (1988, 1998) and is rooted in the idea that every earthquake triggers nearby earthquakes; alternatively, all earthquakes accompany aftershocks. The ETAS model has been further extended to include other features, such as the elliptical spatial distribution of aftershocks (Ogata et al. 2003; Ogata 2004; Zhuang

et al. 2004; Helmstetter and Sornette 2004; Ogata and Zhuang 2006; Chu et al. 2011).

Statistical characteristics of the seismicity are also examined by considering that spatio-temporal distribution of near-field earthquakes (i.e., earthquakes occurring within the classical aftershock zone; van der Elst and Brodsky 2010) is independent of the dimensions of the region under consideration and the magnitudes of earthquakes (Kagan and Knopoff 1980; Corral 2004a; Marekova 2014). For instance, in southern California, where high-quality seismic data are available for several recent decades, both the inter-event distances (distances between earthquakes) and the inter-event times (lapsed time between earthquakes) exhibit statistical distributions involving power-law regimes (Bak et al. 2002; Corral 2004a, b, 2008; Davidsen and Paczuski 2005). Bak et al. (2002) analyzed the seismic catalog for California from 1984 to 2000, by dividing the study region into $L \times L$ grid cells and calling the interval between two consecutive events a waiting time. They then measured the waiting times of pairs of earthquakes with a magnitude larger than the catalog threshold magnitude that occurred within each cell. They found that the distribution of waiting times exhibits a scaling law. Davidsen and Paczuski (2005) used the method of Bak et al. (2002) to evaluate the spatial distances between consecutive seismic events in Southern California. They used earthquake data from 1984 to 2000, giving no constraint on magnitude range or tectonic setting. They found that the distance between two consecutive earthquakes exhibits a power law behavior that depends on the waiting time rather than on the threshold magnitude. Felzer and Brodsky (2006) analyzed the relocated Southern California catalog between 1984 and 2002 to examine the characteristics of the spatial distribution of aftershocks. They indicated that the inter-event distance follows a power-law decay up to a distance of about 50 km and 500 km from the epicenter of mainshocks with magnitudes of 2–4 and of 5–6, respectively.

In contrast to the occurrence of near-field earthquakes, the spatio-temporal characteristics of successive earthquakes that occur in the far-field region (i.e., outside the classical aftershock area) are not yet well understood. To tackle this problem, several studies have attempted to investigate the spatio-temporal occurrence of moderate and large earthquakes in the far-field region using global and regional earthquake catalogs. For example, Gasperini and Mulargia (1989) analyzed earthquake ($M \geq 4.0$) cluster properties in Italy using a regional seismic catalog for the period between 1890 to 1982. Earthquakes were classified as either independent or as members of a given cluster within a specified time–space window. They found that, for an interval time of 14 days to 60 days, the observed seismicity was sufficiently homogeneous within a region ranging from 80 to 140 km, respectively. Lomnitz (1996) investigated the possibility of long-range triggering by analyzing worldwide large shallow earthquakes ($M \geq 7.0$) that occurred during the period 1900 to 1989. He investigated anomalous seismicity immediately after the occurrence of $M \geq 7.0$ earthquakes for a lapsed time of about 1 month. He found that a large earthquake enhances seismic activity in two concentric regions: the aftershock region (0–300 km) and the far-field region (400–1000 km). He noticed that both regions were activated together and separated by a seismicity gap region (300–400 km). Huc and Main (2003) examined the characteristics of earthquake triggering ($M_w \geq 5.0$) by analyzing a global data catalog for the period 1977 to 2000. They computed the interval distances for each pair of source-triggered events, and found no systematic triggering effect beyond 100–150 km, which is almost the thickness of the lithosphere.

It is also known that large earthquakes are sometimes preceded by foreshocks: about 10–20% of the mainshocks with $M_w \geq 6$ are accompanied by foreshocks (Reasenberg 1999). Some foreshocks have a magnitude larger than 6. For example, in Japan, 2 days after an M_w 7.3 earthquake, the 2011 Tohoku–Oki earthquake with magnitude M_w 9.0 occurred along the Pacific plate boundary (Marsan and Enescu 2012); an M_w 6.5 earthquake hit the Hinagu active fault in Kyushu, Japan, on April 14, 2016, and was followed by a large earthquake with M_w 7.3 that took place at Futagawa active fault on April 16 (Goda et al. 2016). In New Zealand, the June 2020 M_w 7.4 earthquake was followed by three large earthquakes with magnitude M_w 7.2, M_w 7.4, and M_w 8.1 on March 3, 2021, within a few hours of each other (U.S. Geological Survey (USGS) 2021). These large earthquakes may be classified as a foreshock of the following mainshock (Utsu 1955), but such a large foreshock exceeding a magnitude of about 6 is generally recognized as a main shock before the occurrence of the following larger earthquake. It is also known that large earthquakes sometimes successively occur, which may not be explained by Båth's law (1965) and may not be attributed to the so-called aftershock activity. For example, in Turkey, six large earthquakes with magnitudes of 7.0–7.8 successively occurred along a 900-km-long zone of continuous surface ruptures along the Anatolian active fault system. The earthquakes migrated in a westward direction from 1939 to 1967 (Barka 1996): The M7.8 Erzincan earthquake in 1939, the M7.1 Erbaa–Niksar earthquake in 1942, the M7.3 Tosya earthquake in 1943, the M7.3 Bolu–Gerede earthquake in 1944, the M7.0 Abant earthquake in 1957, and the M7.1 Mudurnu Valley earthquake in 1967. For 5 years after the 2004 Sumatra earthquake with magnitude M_w 9.2, three large earthquakes with $M_w > 7$ occurred along the boundary

between the Indian oceanic plate and Sumatra Island in Indonesia: the M_w 8.7 Nias earthquake in 2005, which occurred directly south of the rupture area of the Sumatra earthquake, the M_w 8.5 and M_w 7.9 earthquakes that occurred on Sep. 12, 2007, about 130 km southwest of Bengkulu on the southwest coast of Sumatra island and about 185 km south–southeast of Padang in West Sumatra, respectively. These earthquakes are often simply termed triggered earthquakes (Stein 1999; Sevilgen et al. 2012).

These previous studies have quantitatively and systematically examined the occurrence possibility and/or triggering processes of successive earthquakes at global and regional scales. However, most of the previous studies have analyzed a limited range of magnitudes to examine the successive occurrences of earthquakes. In addition, the previous studies from the 1990s or early 2000s could not avoid using a limited number of reliable data, because the worldwide catalog was prepared from 1976. The present study, therefore, analyzes two reliable global and regional earthquake data catalogs to clarify spatio-temporal characteristics of successive earthquakes for a wide magnitude range of M_w 4.0 to $M_w > 7$. We estimate the triggering distance at which successive earthquakes occur, using a method that can be applied even for a large magnitude range with not a large number of earthquakes. We further relate the results of triggering distance with the ETAS model and discuss the occurrences of successive earthquakes.

Data

Global data catalog

We used the data catalog of CMT solutions provided by the Global CMT project run by Columbia University (Dziewonski et al. 1981; Ekström et al. 2012). CMT solutions for earthquakes have routinely been determined from analyses of observed seismic waves recorded at stations deployed around the world. The centroid, occurrence time, and moment magnitude for earthquakes occurring around the world are provided. The data for a period of 40 years from 1977 to 2016 were analyzed in the present study. We used shallow earthquakes that occurred at depths between 0 and 70 km, which are about 80% of all earthquakes within the catalog (Bird et al. 2002). In total, 13,198 shallow earthquakes were analyzed. Because CMT solutions are determined for relatively large earthquakes that excite long-period waves propagating over a long distance, the data catalog is complete for the earthquakes with a magnitude of at least about 5. This can be confirmed from the magnitude frequency distribution that follows the Gutenberg–Richter's relation (e.g., Nishimura 2017). However, using various methods, Mignan and Woessner (2012) found that the Global CMT catalog is complete for magnitude of at least 5.3. Therefore, to examine the averaged features of successive earthquakes in space and time on a global scale, the present study gives attention to earthquakes with a magnitude larger than or equal to 5.5.

Regional data catalog

We used seismic moment tensor catalog data from the Full Range Seismograph Network of Japan (F-net) provided by National Research Institute for Earth Science and Disaster Resilience (NIED) for the analysis of smaller earthquakes that occurred in and around Japan. Kubo et al. (2002) indicated that the NIED F-net catalog is consistent with the global CMT catalog with differences of less than 0.1 in moment magnitude, 10 km in focal depth, and 15° in the orientation of the principal axes. They also showed that the moment tensors are reliably estimated for the earthquakes with a moment magnitude of above 3.5. Earthquakes in the NIED F-net catalog are available since 1997, but high-quality data recorded by the dense NIED F-net only became available from 2001 after the Fundamental Research on Earthquakes and Earth's Interior Anomaly seismographic network was integrated into the seismographic network set up for the KIBAN project (Okada et al. 2004). Furthermore, to avoid the effects of aftershocks of the 2011 Tohoku–Oki earthquake (M_w9.0), we used the earthquake data for the period from 2001 to 2010. To determine the magnitude of completeness (M_c) in the NIED F-net catalog, we use the method of maximum curvature (Wiemer and Wyss 2000). This method defines M_c as the point of maximum curvature of the cumulative frequency–magnitude distribution, which corresponds to the magnitude bin containing the highest frequency of events in the non-cumulative frequency–magnitude distribution. For the data we analyzed, M_c is estimated to be 3.8. However, the completeness magnitude significantly changes when using only earthquakes that occur onshore and/or offshore (Nanjo et al. 2010), or using earthquakes that occur during the daytime or nighttime (Iwata 2013), and/or by the evaluation method (Mignan and Woessner 2012). Considering these previous studies, we analyzed the spatio-temporal behavior of successive earthquakes that occurred around Japan with magnitudes of $4.0 \leq M_w < 5.5$. As with the global CMT catalog, only shallow earthquakes (70 km in depth) were analyzed.

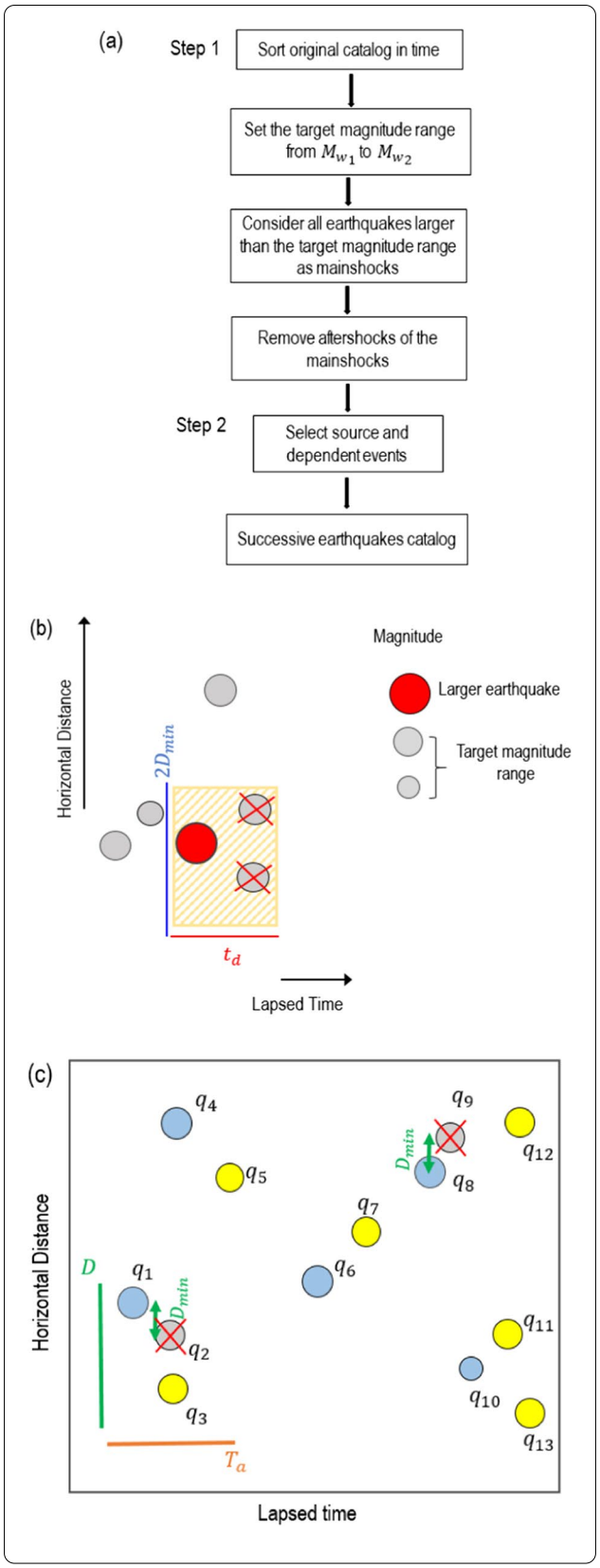

Fig. 1 Schematic illustration of the method. **a** Flowchart of selection of earthquake catalog. **b** Procedure for removal of aftershocks of a large earthquake (Step 1). $D_{\min}$ represents the extent of the aftershock area and t_d represents the duration of the aftershock sequence. **c** Procedure for selection of source and dependent events (Step 2). We select the first earthquake q_1 as a source event (E_0^1) and search for its dependent events q_3. We do not use q_2 as a dependent event, because it occurs within a horizontal distance of $D_{\min}$ from the source event (i.e., it is treated as an aftershock of the source event). The event q_4 is selected as a source event (E_0^2) and q_5 is selected as a dependent event. The event q_6 is a source event (E_0^3) and q_7 is its dependent event. The event q_8 is selected as a source event (E_0^4) with a dependent event q_{12}, but q_9 is not a dependent event. The event q_{10} is a source event (E_0^5) with two dependent events q_{11} and q_{13}

Methods

Identifying successive earthquakes in space and time

The present study focuses on successive earthquakes that may not be classified as so-called aftershocks, and we develop an algorithm for identifying clusters of successive earthquakes in space and time. The algorithm consists of two steps: (1) removal of aftershocks and (2) detection of successive earthquakes (Fig. 1a). These two steps are described in more detail in the following subsections.

Step 1: Removal of aftershocks of large earthquakes

The aftershocks induced by larger earthquakes are removed by applying the following procedure: (a) sort earthquakes in time; (b) set the target magnitude range from M_{w1} to M_{w2}; (c) consider all earthquakes larger than the target magnitude range as mainshocks; and (d) for each selected mainshock, remove all the subsequent events that occurred within a space–time window [$D_{\min}$, t_d] defined in "Parameters used in steps 1 and 2" section, where $D_{\min}$ is the extent of the aftershock zone and t_d the duration of the aftershock sequence following the mainshock. The catalog in which these aftershocks are removed by the procedures in (a)–(d) is called a "sub-catalog" in the present study. Figure 1b schematically illustrates how aftershocks of larger earthquakes are removed in step 1.

Step 2: Selection of source and dependent events

We suppose that successive earthquakes consist of a source event and dependent events that occur closely in space and time. We use the following procedures for each target magnitude range from M_{w1} to M_{w2}: (a) a start time is set to be the beginning time of the sub-catalog; (b) a source event is selected from the sub-catalog in order from the start time, and is termed as E_o^i, where i represents the number of source event; (c) when an earthquake E_o^g larger than E_o^i occurs within an interval time

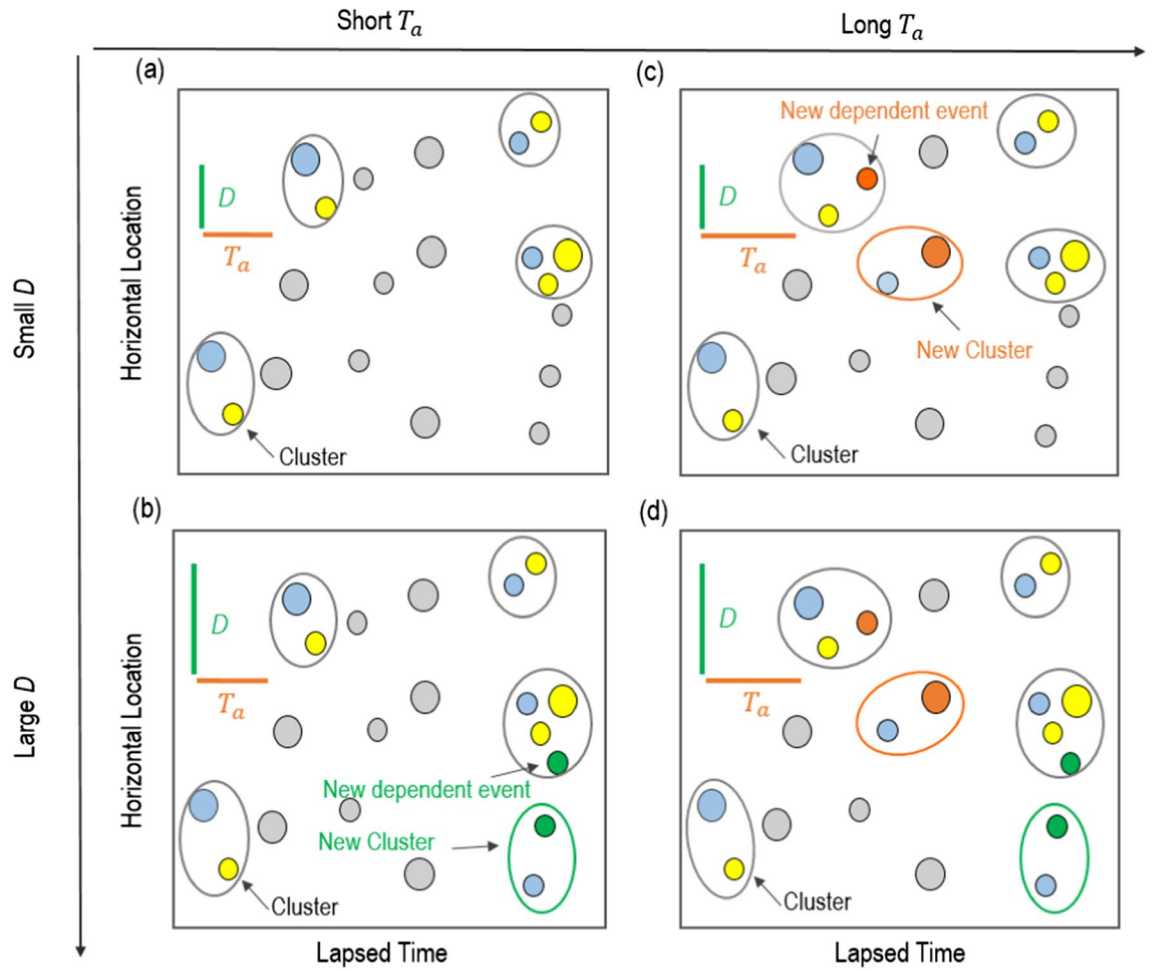

Fig. 2 Schematic illustrations showing how different clusters of successive earthquakes are defined for different choices of D and T_a. Blue circles represent source events, yellow circles mean dependent events, and each gray ellipse indicates a group of successive earthquakes (clusters). **a** Group of clusters obtained for initial D and T_a. **b** Green circles and green ellipse represent new dependent events and a new cluster, respectively, obtained by increasing D. **c** Orange circles and orange ellipse represent new dependent events and a new cluster, respectively, obtained by increasing T_a. **d** New dependent events and new clusters obtained by increasing both D and T_a

of t_b before the occurrence of E_o^i and within a distance of 2 $D_{\min}(E_o^g)$ from the centroid of E_o^i in the sub-catalog, E_o^i is not used as a source event, and we go to step (f); (d) earthquakes occurring within a lapsed time T_a and a horizontal distance D from the source event are searched for, and are defined as dependent events belonging to the "cluster" E_o^i; (e) the start time is set to be just after the occurrence time of the ith source event, and we go to step (b) to select the next source event $(i+1)$ that does not belong to the clusters previously determined; and (f) steps (b) to (e) are repeated until the last earthquake in the sub-catalog is identified. Note that in procedure (d), the earthquakes located within a distance of $D_{\min}$ from the epicenter of E_o^i are not used. Step (c) removes the aftershocks of the mainshock in the target magnitude range.

To avoid double counting, all the identified source and dependent events are removed from further selection so that earthquakes cannot belong to two or more clusters. We define the earthquakes belonging to each cluster as "successive earthquakes." Figure 1c schematically illustrates how to obtain the source events and dependent events using the lapsed time T_a and distance D. As shown in Fig. 2, the number of clusters and/or successive earthquakes changes with the lapsed time T_a and the horizontal distance D. By counting the number of clusters for various values of T_a and D, we clarify the characteristics

of successive earthquakes. Note that there is no notion of foreshock in the analysis (that is, much smaller earthquake triggers a large one), because including such a notion makes the algorithm and interpretation of results complicated.

Parameters used in steps 1 and 2

The time interval, t_b, which is defined as the elapsed time between a targeted source earthquake and the preceding large earthquake in the region, is set to be 14 days, because most of the largest aftershocks occur within 10 days after the occurrence of each mainshock (Utsu 1957). Following Utsu (1955), we obtain the aftershock distance in kilometers, $D_{\min}$, using the following equation: $D_{\min} = c\sqrt{A/\pi}$, where A is the slip area in square kilometers determined from the magnitude of the source event: $\log_{10}A = 1.02M_w - 4.0$. To sufficiently exclude the aftershocks of the source event, we set the coefficient c to be 3. The duration of aftershocks (t_d) is set by examining several large earthquakes occurring in Japan and around the world: 730 days for large earthquakes with $M_w \geq 5.5$ and 1825 days for small earthquakes with $M_w < 5.5$ (see Appendix A2). Because the selection of mainshocks may change the selection of aftershocks (Felzer and Brodsky 2006; Marsan and Lengliné 2010), we examined the effect of c and t_d by changing their values.

Measurement of triggering distance

To examine whether the successive earthquakes selected by steps 1 and 2 randomly occur in space and time, we compared the results obtained from analyses of actual catalog data to those from simulated catalog data. Because the temporal distribution of large earthquakes is well described by a Poisson process when aftershocks are excluded (e.g., Gardner and Knopoff 1974; Michael 2011; Shearer and Stark 2012), we made simulated data catalogs of earthquakes as follows: the centroids and magnitudes were set to be the same as the real data, but the origin times were randomly set during the observation period of the real catalog using a random function in a computer code that can generate random values equally distributed between 0 and 1.

We picked up the successive earthquakes and counted the number of clusters for the simulated data catalogs by applying the same procedure as that used for the real data catalogs. The simulations were done 100 times, and the average number of clusters was calculated. As shown in the following sections, we defined the intersection point, where the number of clusters obtained from real data merges with that obtained from simulated data as "triggering distance."

Results

Analysis of global CMT catalog

To investigate the spatio-temporal distribution of successive earthquakes at the global scale, we divided the earthquakes in the global CMT catalog into five magnitude ranges: $5.5 \leq M_w < 6.0$ (9024 earthquakes), $6.0 \leq M_w < 6.5$ (2863 earthquakes), $6.5 \leq M_w < 7.0$ (907 earthquakes), and $M_w \geq 7.0$ (404 earthquakes). To remove the aftershocks, we set the aftershock duration t_d to 730 days (we also show the results for 365 days and 180 days in Appendix).

We counted the number of clusters for three lapsed times: $T_a = 60$, 180, and 365 days. The horizontal distance, D, from the centroid of the source earthquake changes from 10 to 500 km every 10 km for the first two magnitude ranges ($M_w< 6.0$) and from 100 to 1000 km every 100 km for the other magnitude ranges ($M_w \geq 6.0$). Then, we counted the number of clusters. Figure 3 shows the number of clusters versus the horizontal distance for the three lapsed times. The results show that most of the numbers of clusters increased with increasing lapsed time T_a and with increasing horizontal distance D. However, for the small magnitude ranges of $M_w < 6.5$, the number of clusters decreased in the ranges of large T_a, large D, or both. For example, for $5.5 \leq M_w < 6.0$, the number begins to decrease from 400 km for T_a of 365 days. Such decreases occur, because multiple clusters come together when the horizontal distance is extended and the lapsed time increases (see Fig. 2).

Figure 3 also plots the results obtained for the simulated catalog. The number of clusters for the simulated catalog more rapidly increases with the horizontal distance than the number for the real catalog at short distances, and the former then approaches or becomes equal to the latter. Alternatively, the number of clusters for the real catalog is always larger than the number for the simulated catalog at shorter distances, and merge to those for the simulated catalog at long distances. This result strongly suggests that the earthquakes trigger another or more earthquakes over shorter distances. The first intersection point, where the number of clusters obtained from the real catalog coincides with that obtained with the simulated catalog represents the distance where triggering effect ceases. Hence, we define this distance as the "triggering distance," as explained in "Measurement of triggering distance" section. The triggering distance decreases with the lapsed time, which suggests that the triggering effect gradually diminishes and the seismic activity returns to the normal condition. For example, the triggering distances are 600 km, 500 km, and 240 km at $T_a = 60$, 180, and 365 days, respectively, for $M_w \geq 7.0$. The values are 450 km, 300 km, and 200 km

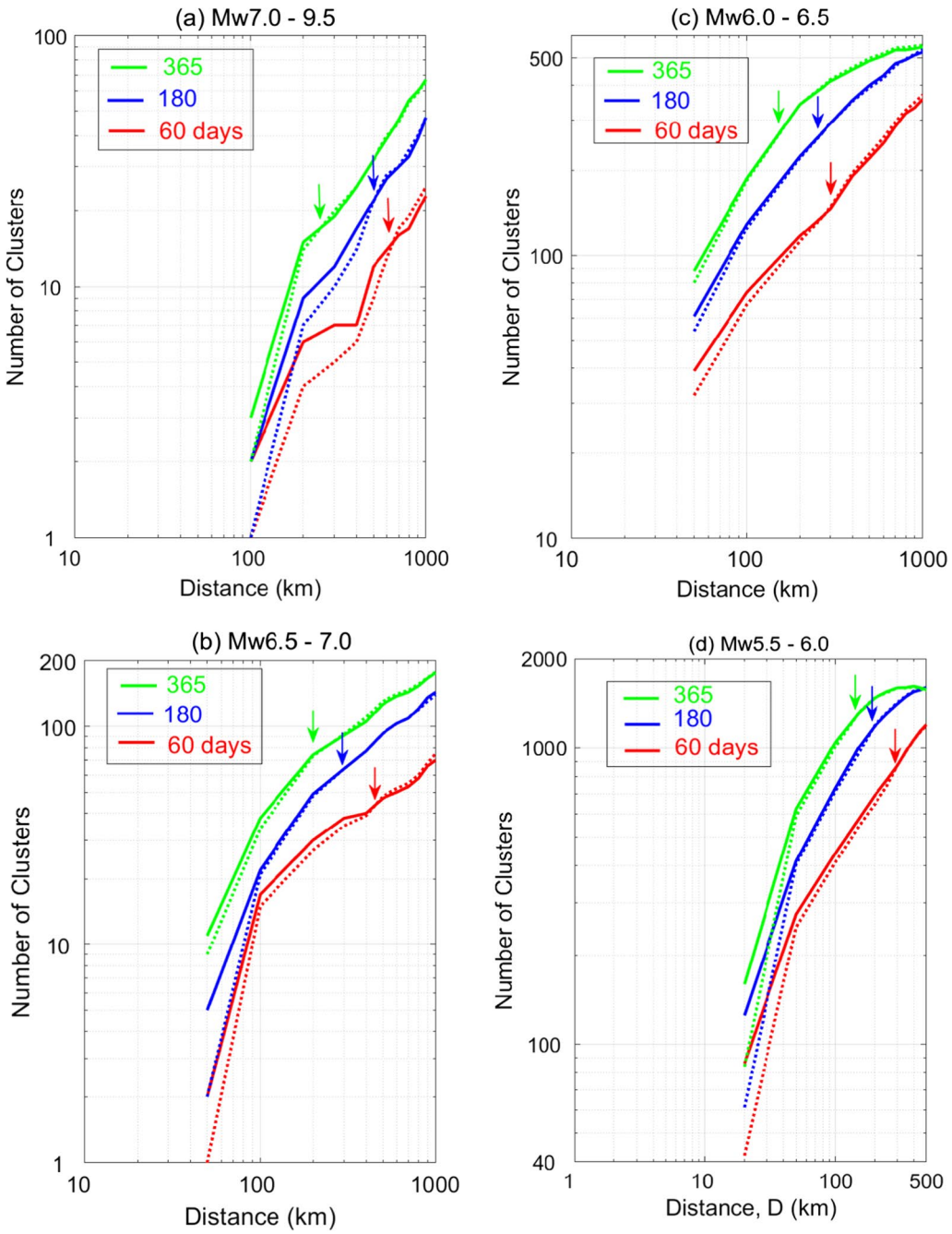

Fig. 3 Number of clusters versus horizontal distance for three lapsed times for the global CMT catalog. Solid lines represent the results obtained from analyses of real data and dotted lines are those from a simulated data catalog. **a** M_w 7.0–9.5, **b** M_w 6.5–7.0, **c** M_w 6.0–6.5, and **d** M_w 5.5–6.0. $c = 3$ and $t_d = 730$ days are used. Arrows indicate the triggering distances (see the text). Note that the ranges of the vertical and horizontal axes are different for (**a**)–(**c**). Note that the vertical axis ranges are different for the four panels to have a better resolution

at 60, 180, and 365 days, respectively, for $6.5 \leq M_w < 7$. The results of different lapsed times are very close to each other although the number of successive earthquakes decreases for the lapse times of 60 ad 180 days. Table 1 summarizes the estimated triggering distances. Table 2 shows the percentages of successive earthquakes that

Table 1 Triggering distances estimated at global (CMT) and regional (NIED F-net) scales

Catalog	Magnitude	Triggering distance (km)		
		60 days	180 days	365 days
CMT	$M_w \geq 7$	600	500	240
	$6.5 \leq M_w < 7$	450	300	200
	$6.0 \leq M_w < 6.5$	300	260	150
	$5.5 \leq M_w < 6.0$	270	190	130
NIED F-net	$5.0 \leq M_w < 5.5$	180	110	60
	$4.5 \leq M_w < 5.0$	90	70	40
	$4.0 \leq M_w < 4.5$	65	45	30

occurred within the triggering distances among all of the observed earthquakes.

The earthquakes occurring within the triggering distance may represent the earthquakes triggered by previous large earthquakes, while the earthquakes beyond the triggering distance can be explained by random occurrence. Note that the earthquakes occurring within the triggering distance potentially include not only the earthquakes triggered by previous large earthquakes but also the randomly occurring earthquakes. However, it is difficult to exactly separate them and evaluate the percentages of successive earthquakes among the background seismicity from our analyses.

Figure 4 shows the locations of successive earthquakes at the global scale for three magnitude ranges at the lapse time of 365 days. Successive earthquakes are distributed along all types of plate boundaries: convergent boundaries, such as subduction zones and collision zones, divergent boundaries (e.g., East African Rift System and ridges) and transform boundaries (e.g., San Andrea fault and Anatolian fault system). Different lapse times also show similar distribution, although the numbers of successive earthquakes come to be smaller.

For each analyzed magnitude range, we also perform the same analysis by counting the number of successive earthquakes instead of clusters. The results in Additional file 1: Figure S1 show a good agreement between the triggering distance obtained by counting the number of clusters and those obtained by counting the number of earthquakes.

Analysis of NIED F-net catalog

To examine whether similar features of successive earthquakes are retrieved for smaller earthquakes, we analyzed the earthquakes occurring around Japan islands using the F-net catalog provided by NIED. Japan is one of the most seismically active regions in the world, and is monitored by a nation-wide dense seismic network operated by the Japan Meteorological Agency (JMA) and NIED (Okada et al. 2004). Its seismic activity may be roughly divided into three types (Taira 2001; Earthquake Research Committee 2020). The first is the earthquakes that occur on and around the plate boundaries, which result from the subduction of two plates: the Pacific Plate under the land plate from the Kuril, Japan, and the Izu–Bonin Trenches; Philippine Sea Plate under the land plate at the site of the Nankai Trough and the vicinity of the Nansei Islands (Ryukyu) Trench. The second is the shallow earthquakes that occur beneath inland regions of Japan. The third is the earthquakes occurring in the eastern margin of the Sea of Japan.

We divided the earthquakes in the catalog into four magnitude ranges: $4.0 \leq M_w < 4.5$ (3297 earthquakes), $4.5 \leq M_w < 5.0$ (1036 earthquakes), and $5.0 \leq M_w < 5.5$ (342 earthquakes). To remove the aftershocks, we set the aftershock duration to 1825 days (we show the cases for 730 and 365 days in Appendix). The number of clusters is calculated for three lapsed times: $T_a = 60$, 180, and 365 days. The horizontal distance, D, from the centroid of the source earthquake changes from 10 to 300 km every 10 km for the magnitude ranges of $4.5 \leq M_w < 5.0$ and $5.0 \leq M_w < 5.5$ and from 5 to 100 km about every 10 km for the magnitude ranges of $4.0 \leq M_w < 4.5$.

Figure 5 shows the number of clusters versus the horizontal distance, where solid lines represent the number

Table 2 Ratio of number of events within triggering distances to the total number of events in the catalog

Catalog	Magnitude	Total number of earthquakes in the catalog	Ratio (%)		
			60 days	180 days	365 days
CMT	$M_w \geq 7$	404	6.4	9.7	8.4
	$6.5 \leq M_w < 7$	907	9.2	14.9	18.2
	$6.0 \leq M_w < 6.5$	2863	14.5	20.9	23.5
	$5.5 \leq M_w < 6.0$	9024	20.2	32.1	31.5
NIED F-net	$5.0 \leq M_w < 5.5$	370	11.6	18.6	14.8
	$4.5 \leq M_w < 5.0$	1206	6.4	9.5	9.8
	$4.0 \leq M_w < 4.5$	3333	3.6	5.1	4.9

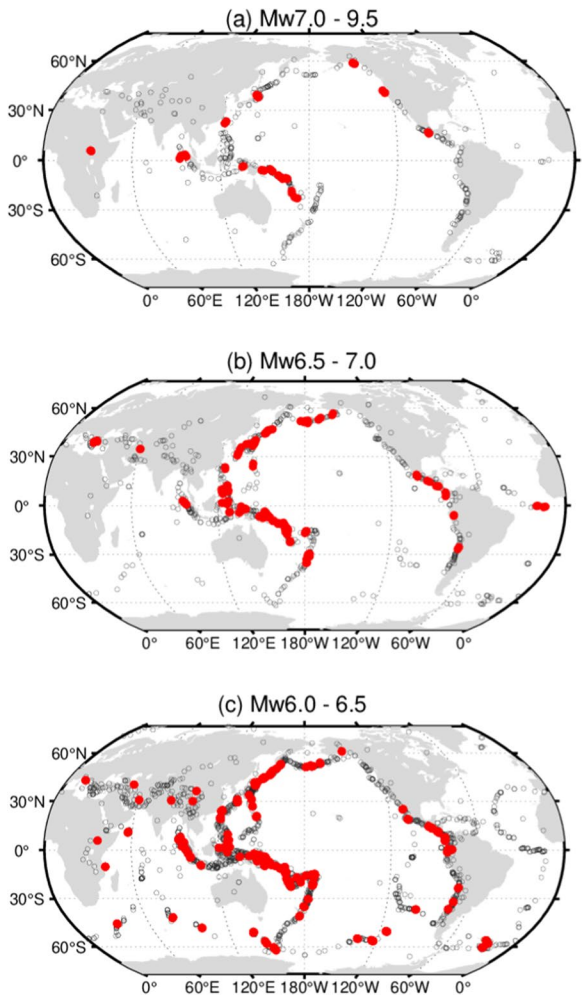

Fig. 4 Spatial distributions of successive earthquakes for **a** $M_w \geq 7.0$, **b** $6.5 \leq M_w < 7.0$, and **c** $6.0 \leq M_w < 6.5$. Red dots represent earthquakes occurring within the triggering distances at a lapsed time of 365 days. Black open circles represent the earthquakes reported in the global CMT catalog

of clusters for the real data catalog, while dotted lines are for the simulated catalog. The number of clusters increases with increasing lapsed time and with increasing horizontal distance except for the cases of smaller magnitude ranges at large T_a and/or large D, which are the same as the results for the global CMT catalog. Table 1 summarizes triggering distances for all the magnitude ranges at different lapsed times, and Table 2 shows the percentages of successive earthquakes at the triggering distance to the total number of earthquakes. No significant differences are observed in terms of the percentages of successive earthquakes for various lapsed times within the magnitude ranges. On the other hand, the percentages of successive earthquakes decrease with decreasing magnitude. This may be because small earthquakes occur more frequently than large earthquakes, and a large aftershock duration leads to the removal of a significant number of aftershocks in small magnitude ranges than in larger ranges, where earthquakes occur at quite large time intervals.

The spatial distribution of successive earthquakes is in good agreement with the main tectonic features of seismic activity in and around the Japanese islands (Fig. 6). Successive earthquakes are observed for 643, 37, and 3975 earthquakes with $4.0 \leq M_w < 5.5$ that occurred beneath the inland areas of Japan, the Sea of Japan, and along plate boundaries, respectively. During the analysis period from 2001 to 2010, the percentages of successive earthquakes to the total number of earthquakes at the plate boundaries are about 2% (91 events) along the Kuril trench, about 1% (48 events) along Japan, 1% (47 events) along Izu–Ogasawara, and 3% (122 events) along Nansei island trenches at $T_a = 365$ days. No successive earthquakes are observed along the Nankai Trough, probably because of low seismicity along this trough (e.g., Nakano et al. 2013). For earthquakes that occurred beneath the inland areas of Japan and Sea of Japan, we find that the percentages of successive earthquakes are about 2% (14 events) and 0% (0 events), respectively. We find that 7 successive earthquakes beneath the inland areas of Japan (Hokkaido, Kanto, and Chugoku areas) occurred in the region within a distance of 50 km active faults (Nakata and Imaizumi 2002) for a lapsed time of 365 days, while no earthquake occurred within 50 km from the summit of active volcanoes (Fig. 6) (Japan Meteorological Agency 2013). Although the number of successive earthquakes is small, successive earthquakes tend to be located close to active faults.

Discussion

Comparison of the triggering distance estimated from global and regional catalogs

To quantitatively evaluate the characteristics of triggering distance, we analyzed its dependence on the seismic moments of the source events. Figure 7 plots the triggering distances versus the seismic moment M_0. Results both for the global CMT catalog and NIED F-net catalog are shown together. The seismic moment for each data is calculated from the moment magnitude averaged for all the earthquakes in each magnitude range using the equation $M_w = (2/3)(\log_{10} M_0 - 9.1)$ (Kanamori and Anderson 1975; Hanks and Kanamori 1979; Bormann and Giacomo 2010).

The triggering distance almost increases in proportion to the seismic moment on the double logarithmic graphs

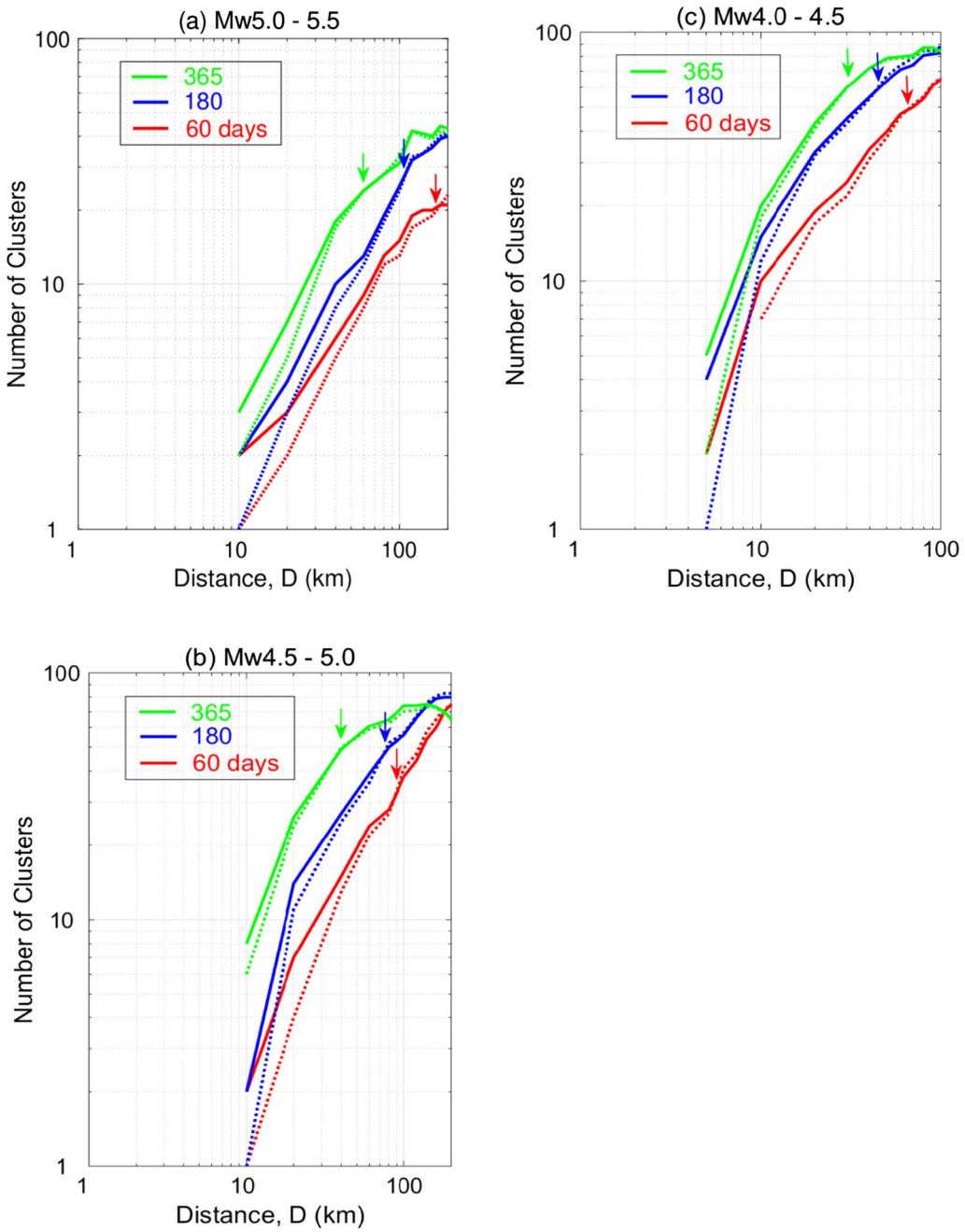

Fig. 5 Number of clusters versus horizontal distance for three lapsed times for the NIED F-net catalog. Solid lines represent the results obtained from analyses of real data and dotted lines are those from a simulated data catalog. **a** M_W 5.0–5.5, **b** M_W 4.5–5.0, and **c** M_W 4.0–4.5. $c = 3$ and $t_d = 1825$ days are used. Arrows indicate the triggering distances (see the text). Note that the ranges of the horizontal axes are different for (**a**)–(**c**)

for all three lapsed times. The triggering distances estimated from the global CMT are fairly well aligned with those from NIED F-net data. We fit a regression line expressed by $\log_{10} D = a_h \log_{10} M_0 + b_h$ to the results for both catalogs together. We estimated a_h to be about 1/5 to 1/4 for the three lapsed times, which are slightly smaller than the value of 1/3 that is derived from the scaling relation of static stress changes to the seismic moment. The time dependence of triggering distances is plotted on a double logarithmic scale in Fig. 8a, c and a semi logarithmic scale in Fig. 8b, d. It is clearly recognized that the triggering distances decay with a similar

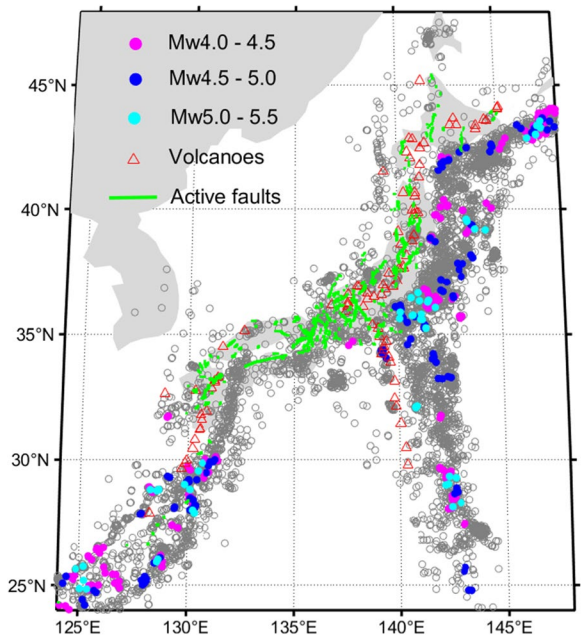

Fig. 6 Spatial distributions of successive earthquakes evaluated at a lapsed time of 365 days in Japan. Color circles represent successive earthquakes. Green lines represent active faults and open red triangles are active volcanoes. Gray open circles represent the earthquakes reported in the F-net catalog

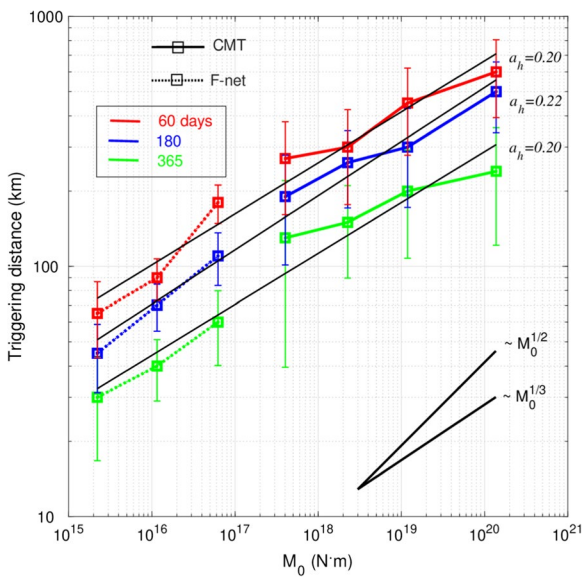

Fig. 7 Relation between the triggering distances and seismic moment (M_0). The results obtained from analyses of global CMT and NIED F-net catalogs are represented by solid and dashed lines, respectively. Vertical lines are error bars of one standard deviation estimated from 100 simulated catalogs. Black straight lines are the regression lines fitting both the results from CMT and NIED F-net catalogs. a_h represents the coefficient expressing the slope

trend for all magnitude ranges. The data are more likely to exponentially decay in time with a characteristic time τ of about 420 to 450 days for the global CMT and NIED F-net catalog (Fig. 8d), although the power law (i.e., logarithmic scale) may explain the data within the error ranges (see Appendix A1).

The scaling law between the triggering distance and seismic moment and the time dependence of the triggering distance were also retrieved by changing the values of t_d and c (see Appendix A2). These results suggest that the triggering distance is a stable parameter that is little affected by the aftershock activity.

Triggering distance for others ranges of magnitudes

We also perform the same analysis by changing the magnitude window for all the earthquakes of magnitudes M_w larger than or equal to 5.5 ($M_w \geq 5.5$, $M_w \geq 6.0$, $M_w \geq 6.5$, and $M_w \geq 7.0$) for global CMT catalog and magnitudes M_w in the range of $4.0 \leq M_w < 5.5$, $4.5 \leq M_w < 5.5$, and $5.0 \leq M_w < 5.5$) for F-net catalog. Additional file 1: Figure S2 shows the triggering distances versus the seismic moment M_0 for the global CMT and NIED F-net catalogs, respectively. It can be clearly seen that changing the magnitude window does not impact the main features of the triggering distance. Note that the seismic moment for each window is mainly determined from the number of small earthquakes.

Relation to ETAS model

The spatio-temporal ETAS model by Ogata (1998) has been considered as a benchmark model to describe the earthquake clustering process, and it has been extensively studied in the context of earthquake short-term clustering (e.g., Console et al. 2007; Marzocchi and Lombardi 2008; Zhuang et al. 2011). In the present study, therefore, we examine whether the ETAS model can explain the characteristics of the observed triggering distance. We first introduce the ETAS model briefly, and then we describe the calculation of the triggering distance in and around the Japan islands using the data that are simulated by the ETAS model. Then, we compare the parameters for the ETAS model with the relations between the triggering distance and seismic moment we obtained in "Comparison of the triggering distance estimated from global and regional catalogs" section.

The ETAS model treats earthquake occurrence as a point process in space and time, and magnitude kernels are typically assumed to be independent; in other words, any event can trigger its own offspring events (Ogata 1998; Zhuang et al. 2004; Ogata and Zhuang 2006). The conditional seismic intensity λ of earthquakes with a

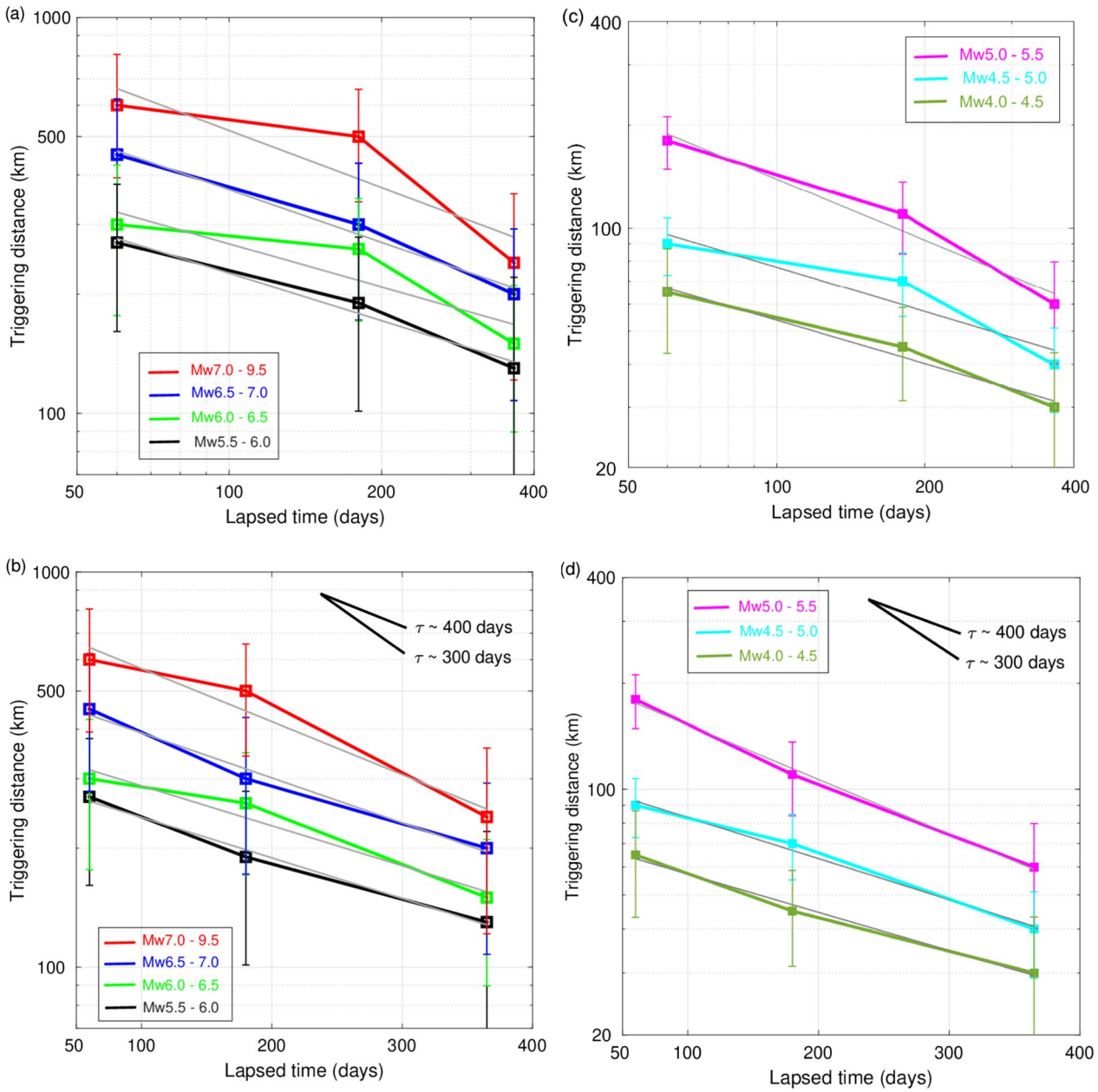

Fig. 8 Relation between triggering distances and lapsed times for global CMT (**a**, **b**) and NIED F-net catalogs (**c**, **d**). Panels (**a**, **c**) show double logarithmic scales, and **b**, **d** show semi-logarithmic scales. Colored dots represent the estimated triggering distances with error bars. Gray lines are the regression lines. τ is the characteristic time of exponential decay

magnitude of M at a position (x, y) and a time t when assuming an isotropic spatial clustering is written as

$$\lambda(x,y,t) = \mu(x,y) + \sum_{i;t_i<t} \nu(t-t_i)g(x-x_i, y-y_i; M_i) \tag{1}$$

where

$$\nu(t-t_i) = K/(t-t_i+c)^p \tag{2}$$

and

$$g(x-x_i, y-y_i; M_i) = e^{(\alpha-\gamma)(M_i-M_c)}\{[(x-x_i)^2 + (y-y_i)^2]/e^{\gamma(M_i-M_c)} + d\}^{-q}. \tag{3}$$

In Eq. (1), $\mu(x,y)$ represents the background seismicity rate, $\nu(t-t_i)$ represents the earthquake occurrence rate and $g(x-x_i, y-y_i; M_i)$ represents the location distribution of the triggered events. In Eq. (2), K measures the productivity of the aftershock activity just after the mainshock and c and p are the parameters of modified Omori's law (Ogata 1998, 2004; Ogata et al. 2003; Kumazawa and Ogata 2014). The parameters in Eq. (3) are as follows: M_c is the cutoff magnitude, α, γ, d, and q are constant parameters characterizing the space–timepoint-process model that may be estimated by maximizing the log-likelihood function, and $t_i < t$ represents the history of the process up to time t. Parameter d (units : degree^2) represents the characteristic triggering distance which prevents a singularity at distance 0, (x_i, y_i) represents the epicenter coordinates of the parent event of magnitude M_i, (x,y) is the centroid of the offspring, α (magnitude^{-1}) represents the efficiency of earthquakes in triggering offspring as a function of magnitude M_i, q describes how triggered events decay in space, and $e^{\gamma(M_i-M_c)}$ scales the size of the M_c aftershock zone with the magnitude of the parent event (Seif et al. 2017).

Analyses of ETAS catalog

We prepared data catalogs in which earthquakes follow the ETAS model, which is called the ETAS catalog hereafter, and estimated the triggering distance. We first calculated seismicity rates at a target region using the following equation presented by Catalli et al. (2008)

$$r = \frac{1}{\Delta T S_{\mathrm{tot}}} \frac{M_0^{\mathrm{tot}}}{M_0^*} \frac{1.5-b}{b} \frac{1}{\left[10^{(1.5-b)(M_{\max}-M_{\min})}-1\right]}, \tag{4}$$

where ΔT represents the duration of the catalog, S_{tot} the area of the studied region, $M_{\max}$ is the maximum magnitude within the catalog, $M_{\min}$ is the minimum magnitude of earthquakes in the catalog, M_0^* is the seismic moment of $M_{\min}$, M_0^{tot} is the total seismic moment in $[M_{\min}, M_{\max}]$, and b is the b value of the Gutenberg–Richter relation.

We used the NIED F-net catalog from 1997 to 2010 and calculated the seismicity rate r for every $0.5^\circ \times 0.5^\circ$ grid cell in and around Japan, assuming a constant b value of 1.1 for all grid cells and $\Delta T = 14$ years. It is more realistic to set b values changing in space and time according to the observed results (Enescu and Ito 2003; Nanjo and Yoshida 2021; Chiba 2022). However, such a spatially changing distribution may make it harder to interpret the results so we use a constant b value. Note that the results for different b values (0.9, 1.0, and 1.4) are similar to the case of $b=1.1$. We assumed that the background seismicity, μ, is 40% of the seismicity rate, r, following the previous studies at California (Gardner and Knopoff 1974; Hardebeck et al. 2008). It is more appropriate to use the background seismicity in Japan, but we do not find a suitable one for such a tectonically complex region. Hence, we tentatively use this value as an average. We used the average ETAS parameters in Japan that are shown in Table 1 of Ogata and Zhuang (2006). We then used the RunAftSimulator.m program to make synthetic ETAS catalogs (Felzer et al. 2002; Hardebeck et al. 2008). Spatial clustering of aftershock activity is also taken into account using an assumption similar to that in Felzer and Brodsky (2006), where the distance distribution of aftershocks follows a power-law decay represented as $\rho \sim d^{-n}$, where ρ is the linear aftershock density at distance d from the main shock and n is a constant. Here, we use $n=1.35$, as obtained by Felzer and Brodsky (2006), and d is between 0.001 and 500 km after Hardebeck et al. (2008). Note that the values of parameter n vary from 1 to 2 encompassing those observed in California and Japan (Richards-Dinger et al. 2010).

We set the time period of the ETAS catalog to be the same as that for the NIED F-net catalog (i.e., from 2001 to 2010). We prepared ten ETAS catalogs in which 2536 events, 811 events, and 250 events on average were generated for M_w 4.0–4.5, M_w 4.5–5.0, and M_w 5.0–5.5, respectively. The total number of earthquakes in the ETAS catalogs does not exactly match the number of earthquakes in the NIED F-net catalog, but this is not important, because the following results are related to the spatio-temporal distribution of events and not to the total number of events in the catalog. As shown in Additional file 1: Figure S4, the RunAftSimulator.m program generates an approximately similar spatial distribution of earthquakes with the NIED F-net catalog data.

We calculated the number of clusters and estimate the triggering distance using the same method shown in "Methods" section. For each ETAS catalog, we prepared 20 simulated data catalogs in which origin times are randomly changed, and obtained the average number of clusters to estimate the triggering distance. The triggering distances were averaged for the results of the ten ETAS catalogs (Additional file 1: Figures S5–S7). Figure 9a shows the relation of the average triggering distances to the seismic moment. The slope is estimated to be about 0.2. Figure 9b shows the lapsed time dependence of the triggering distance. The triggering distances almost exponentially decay with a time constant τ of about 311 days. These results are well matched with those for the NIED F-net catalog, suggesting that the successive earthquakes are explained by the seismicity described by the ETAS model. In addition, the AftSimulator.m program that is used here for synthetic ETAS catalogs generates

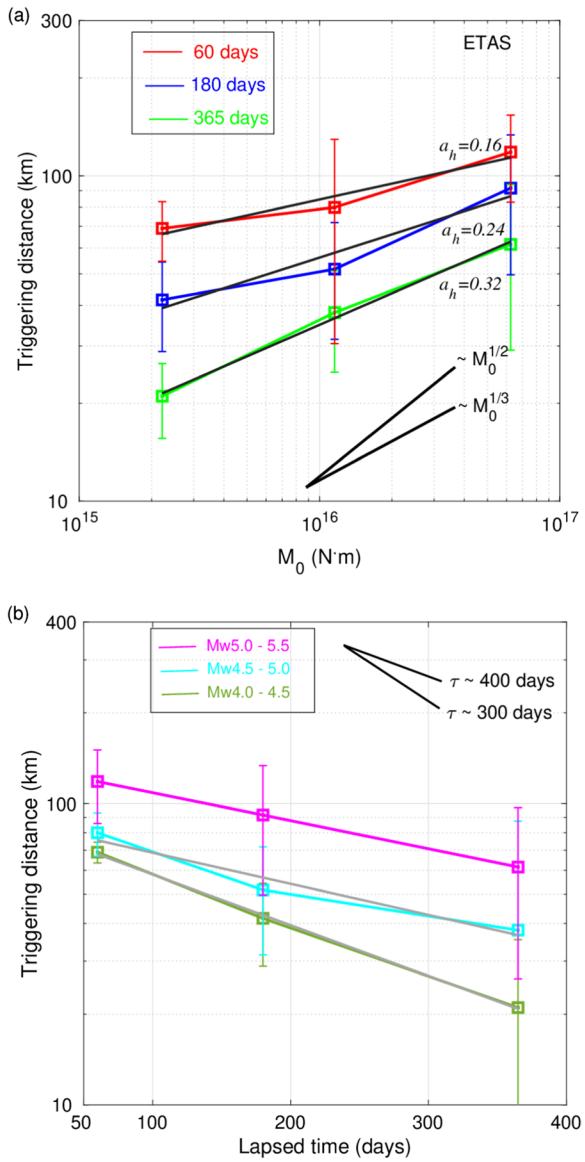

Fig. 9 **a** Relation between triggering distances and seismic moment (M_0) for the synthetic ETAS catalog. Vertical lines are error bars of one standard deviation estimated from 20 simulated catalogs. Black straight lines are regression lines. a_h represents the coefficient expressing the slope. **b** Relation between triggering distances and lapsed times on a semi-logarithmic scale. Colored dots represent the estimated triggering distances with error bars. Gray lines are the regression lines. τ is the characteristic time of exponential decay

background seismicity and aftershocks so that we have the benefit of knowing which events are the background and which are the triggered. Thus, instead of using our declustering method as described in "Methods" section, we use this knowledge in the aftershock removal step and obtain catalogs of background earthquakes. We find that ETAS declustering tends to remove many earthquakes. On average, about 62% of earthquakes were identified as aftershocks by the ETAS declustering method. This high percentage is due to the fact that ETAS declustering accounts for secondary triggering. For each background catalog, we prepared 20 simulated data catalogs in which origin times are randomly changed and measured the triggering distance. However, since the generated background catalogs come from a random process, about 50% of the curve of the cluster number versus the distance for simulated catalog does not merge with that for the background one. This is contrary to the cases for the real data, in which 90% of the curves merge. These results suggest that the triggering process at long distances is related to the aftershock activity.

Estimation of triggering distance using ETAS parameters

Here we explain the power law between the triggering distance and seismic moment shown in Fig. 7. Following Chu et al. (2011), we assume that the term $(x-x_i)^2+\left(y-y_i\right)^2$ in Eq. (3) represents the distance from a given mainshock to generate its offspring earthquakes (i.e., triggering distance, D):

$$D^2=(x-x_i)^2+\left(y-y_i\right)^2 \tag{5}$$

We suppose that the triggering distance is determined by, for example, additional stress caused by a large earthquake. As a result, D can be related to the seismicity rate h, which is the second term on the right-hand side of Eq. (1):

$$h\left(x,y,t\right)=\nu(t-t_{\mathrm{s}})g\left(x-x_{\mathrm{s}},y-y_{\mathrm{s}};M_{\mathrm{s}},D\right), \tag{6}$$

where s represents a source event. When analyzing seismic activity at the global scale, it may be preferable to use the anisotropic spatial distribution of earthquakes to account for the sphericity of the Earth (Ogata 1998, 2004; Ogata et al. 2003; Chu et al. 2011). However, here we use the isotropic spatial distribution assumption for the hypocenters for simplicity.

Parameter d in Eq. (3) is introduced to avoid a singularity in the function g, and the triggering distance is several tens of kilometers. Hence, assuming $d \ll D$, we relate the function $h\left(x,y,t\right)$ to D by

$$D=h^{-1/2q}K^{1/2q}e^{\frac{(M_{\mathrm{s}}-M_{\mathrm{c}})(\gamma q+\alpha-\gamma)}{2q}}(t-t_{\mathrm{s}}+c)^{-p/2q}. \tag{7}$$

Substituting the equation relating the seismic moment with the moment magnitude (Hanks and Kanamori 1979), which is expressed as

$$M_w=(2/3)(\log_{10}M_0-9.1), \tag{8}$$

into Eq. (7), we obtain the following equation:

Table 3 ETAS parameters evaluated in various regions by previous studies

Region	K_0	C (days)	α	γ	p	d(degree^2)	q	M_i	M_c
Japan	0.988×10^{-4}	0.840×10^{-2}	1.962	1.326	0.910	0.203×10^{-2}	1.570	8.4	4.5
	0.171×10^{-4}	0.520×10^{-2}	0.935	0.740	0.961	0.403×10^{-3}	1.408	8.4	4.0
	0.290×10^{-3}	0.748×10^{-2}	1.154	0.891	0.911	0.552×10^{-2}	1.524	8.4	5.0
California	0.51	0.004	1.27	1.31	1.09	1.868×10^{-5}	1.59	7.5	3.5
China	0.2285	0.2663	1.7627	0.5587	1.2363	9.179×10^{-4}	2.1249	7.9	4.0
	0.0588	0.3049	2.3378	1.7503	1.1785	0.519×10^{-4}	1.7864	7.9	4.0
Italy	4.7×10^{-2}	0.012	1.2	0.36	1.11	5.662×10^{-3}	1.57	6.3	2.5

Japan: Tohoku region, Western and Central Honshu, and all Japan from the top to the bottom (Ogata and Zhuang 2006) (Table 1, model 10)

California: southern California (Seif et al. 2017) (Table 2, sets 1)

China: Sichuan province (Guo et al. 2015) (Table 1, Model 3 and 4)

Italy: Central Italy (Lombardi 2016) (Table 1, INGV Bulletin)

Table 4 Predicted value of the slope for the average ETAS parameters estimated at different tectonic settings around the globe

Region	Slope (a_h)	Source
Tohoku	0.25	Ogata and Zhuang (2006)
C&W Honshu	0.13	
All Japan	0.15	
California	0.19	Seif et al. (2017)
Sichuan (model 3)	0.16	Guo et al. (2015)
Sichuan (model 4)	0.30	Guo et al. (2015)
Italy	0.13	Lombardi (2016)

$$\log_{10} D = a_h \log_{10} M_0 + b_h, \tag{9}$$

where

$$a_h = \frac{1}{6.91q}(\gamma q + \alpha - \gamma), \tag{10}$$

$$\begin{aligned} b_h = &- \frac{1}{4.61q}(6.1 + M_c)(\gamma q + \alpha - \gamma) \\ &- \frac{1}{2q}\left[\log_{10}(h) - \log_{10}(K) \right. \\ &\left. + p\log_{10}(t - t_s + c)\right]. \end{aligned} \tag{11}$$

From Eq. (11), the seismicity rate is represented by

$$\begin{aligned} \log_{10}(h) = &\log_{10}(K) - p\log_{10}(t - t_i + c) \\ &- 2qb_h - 0.4(6.11 + M_c)(\gamma q + \alpha - \gamma). \end{aligned} \tag{12}$$

The parameters a_h and b_h in Eqs. (10) and (11) are expressed only by ETAS parameters. Using ETAS parameters at various regions reported in previous studies (Table 3), we calculated a_h in Eq. (10) for Japan (Tohoku region, Central and Western Honshu, and all of Japan) (Ogata and Zhuang 2006), California (Seif et al. 2017), China (Sichuan Province) (Guo et al. 2015), and Italy (Lombardi 2016). The results summarized in Table 4 show that predicted a_h values are estimated to be about 0.1–0.3 for these regions. Large a_h are estimated for Tohoku and Sichuan, where large α and γ are obtained, as predicted from Eq. (10) for $q \geq 1$. These predicted a_h values match pretty well with those obtained from the real data in Fig. 7: 1/5 to 1/4. This consistency between the observed and predicted a_h values imply that clustering of successive earthquakes in space and time is well explained by the ETAS model.

Triggering mechanisms

Several mechanisms have been proposed to explain the spatio-temporal clustering of earthquakes. Static stress changes caused by deformation in the vicinity of a large earthquake may cause Coulomb stress changes on seismic fault planes (i.e., King et al. 1994; Stein 1999; Hardebeck et al. 1998; Freed 2005; Toda et al. 2011a, b). Viscoelastic relaxation, which is caused by viscous flow in the lower crust or upper mantle after the occurrence of a moderate to large earthquake may also change the stress condition of the fault plane (e.g., Freed and Lin 2001). Large earthquakes may cause crustal fluids to migrate, generating fluid pore diffusion. Such processes may decrease the effective normal stress on seismic faults in the crust or plates and lead to the triggering of other earthquakes (Sibson et al. 1975; Sibson 1981; Hickman et al. 1995). Dynamic stress changes associated with the passage of seismic waves excited by a large earthquake are also another possible mechanism to trigger earthquakes at larger distances (e.g., Gomberg and Johnson 2005; Felzer and Brodsky 2006). Dynamic stress change has been used at various regions to explain far-field triggering, such as: in the United States (Hill et al. 1993; Prejean

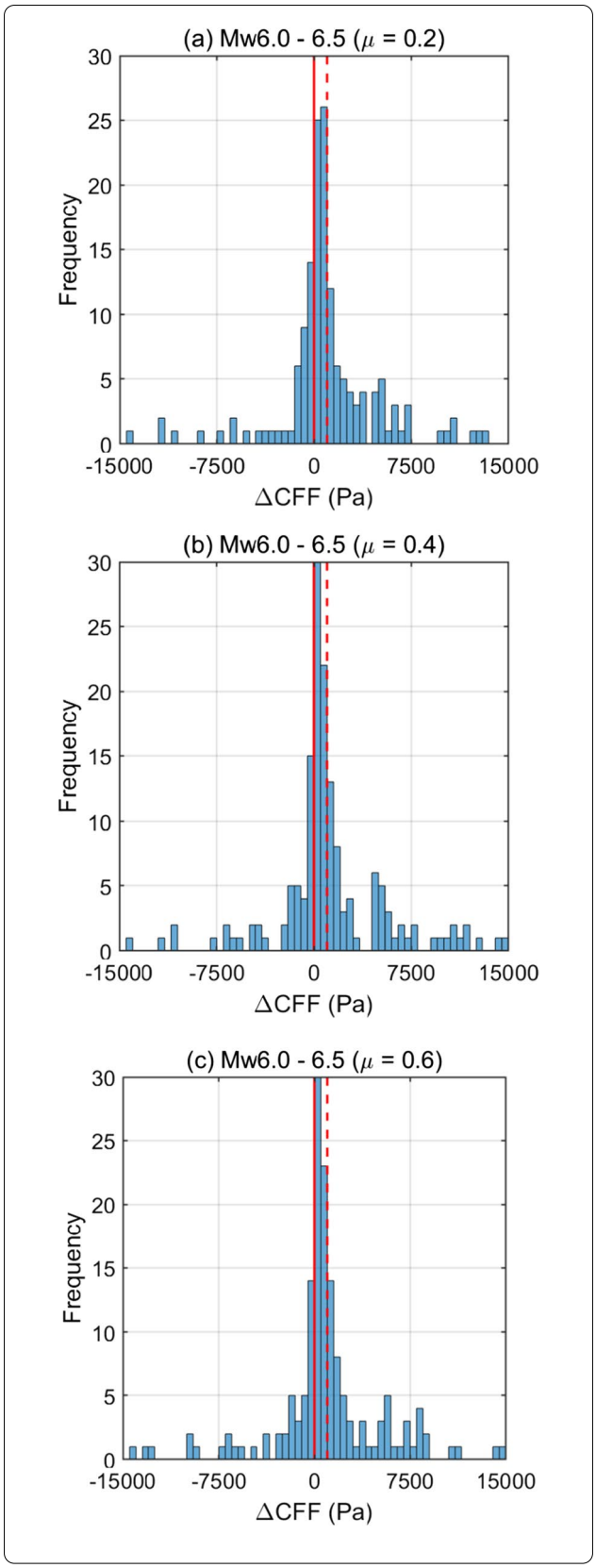

Fig. 10 Example of frequency distribution of Coulomb stress change, ΔCFF, calculated on the fault plane for earthquakes with M_w 6.0–6.5 range. **a** $\mu' = 0.2$, **b** $\mu' = 0.4$, and **c** $\mu' = 0.6$. The red solid lines indicate a threshold stress of 0 Pa and the red dotted lines 10^3 Pa

et al. 2004), Tonga island (Tibi et al. 2003), and Iceland (Arnadottir et al. 2004). Successive earthquakes are found to occur several tens of kilometers away from the source events, and the passage of seismic waves seems to be a more plausible triggering mechanism. Seismic activity dynamically triggered at a given location begins not only with the arrival of P waves from the source event but during or after the arrival of the large-amplitude Love or Rayleigh waves (Hill and Prejean 2006).

The obtained relations of the triggering distance with the seismic moment and lapse time may not directly reveal the mechanism of successive earthquakes. However, we examine the Coulomb stress changes caused by large earthquakes as one of the possible mechanisms. Although the triggering distances we estimated are up to about 500 km and this mechanism is often used to identify the triggering mechanism of nearby large earthquakes through various case studies (Hardebeck et al. 1998; Toda et al. 2008; Ishibe et al. 2017).

The change in the Coulomb failure function (ΔCFF) is defined as $\Delta\mathrm{CFF} = \Delta\tau + \mu'\Delta\sigma$, where $\Delta\tau$ is the shear stress change, $\Delta\sigma$ is the normal stress change, and μ' is the apparent coefficient of friction (e.g., Reasenberg and Simpson 1992). We calculated ΔCFF for two nodal planes of a dependent event using a moment tensor solution of its source event. We calculated ΔCFF using the Coulomb3.3 program provided by the US Geological Survey (https://www.usgs.gov/software/coulomb-3). Because the global CMT catalog only provides a moment tensor solution assuming a point source, we assume the appropriate fault length, L, and width, W, of a source event using an empirical relation for the magnitude and fault size presented in Wells and Coppersmith (1994): $L = 10^{-2.44+0.59M_w}$ and $W = 10^{-1.01+0.32M_w}$. We made all calculations in an elastic half-space with a shear modulus of 32 GPa and a Poisson's ratio of 0.25. The source is assumed to be the source event of each cluster and the receivers are all dependent events belonging to that cluster. We examined 0.2, 0.4, and 0.6 as the coefficient of friction, because many various case studies indicate that the value of $\mu' = 0.4$ yields strong correlations between earthquake occurrence and the ΔCFF. ΔCFFs were calculated for both nodal planes determined from the centroid moment tensor solution. Here we used a nodal plane that shows a larger ΔCFF.

Figure 10 shows an example of the frequencies of ΔCFF for $\mu' = 0.4$. ΔCFF tends to be widely distributed and most values are distributed around 0 Pa. For a threshold stress of 10^3 Pa, which is tentatively set by considering the tidal effect (Tanaka et al. 2002a, b), the percentage of dependent events that satisfy the triggering condition is less than 40% for magnitudes larger than 6: the percentages are 28%, 30%, and 30% at $M_w \geq 7.0$; 28%, 28%, and 24% at $6.5 \leq M_w < 7.0$; and 37%, 37%, and 36% at $6.0 \leq M_w < 6.5$ for $\mu' = 0.2, 0.4$, and 0.6, respectively. When we set the threshold at 0 Pa, the percentages increase to be larger than about 60%: for $\mu' = 0.2, 0.4$, and 0.6, they are 74%, 74%, and 71% at $6.0 \leq M_w < 6.5$; 72%, 69% and 59% at $6.5 \leq M_w < 7.0$; and 63%, 67% and 61% at $M_w \geq 7.0$, respectively. Note that the earthquakes for which we analyze ΔCFF, which are earthquakes within the triggering distance, include earthquakes that randomly occur, as described in "Analysis of global CMT catalog" section. Considering the magnitude range $M_w \geq 7.0$, the 67% of successive earthquakes located in regions with positive ΔCFF represent about 6% of the total number of earthquakes for $M_w \geq 7.0$. This is almost same as the percentage of 8% estimated by Parsons (2002), who analyzed global CMT earthquakes with $M_w \geq 7.0$, supposing that the triggering mechanism is shear stress increase on the fault plane.

The estimated percentages of the dependent earthquakes located in positive ΔCFF may support that static stress change generated by a source event is the triggering mechanism. However, it is noteworthy to mention again that the triggering distance is proportional in logarithmic scales to the seismic moment with a power of 1/5 to 1/4, which is smaller than the value of 1/3 that is derived from the scaling relation of static stress changes to the seismic moment. Therefore, the successive earthquakes may be generated not only by such static strain but also by other mechanisms.

Comparison of triggering distance with the results in previous studies

The triggering distances estimated in this study are in good agreement with those from previous studies. For instance, Lomnitz (1996) searched for events that occurred within a space–time window from the occurrence of any $M \geq 7.0$ mainshocks in a worldwide earthquake catalog. He found that earthquakes with a magnitude $M \geq 7.0$ were triggered at the distance ranging from 300 to 1000 km. Parsons (2002) analyzed earthquakes with $M_s \geq 7.0$ in the global CMT catalog and calculated the shear stress change between source events and dependent events that occurred within a distance of $\pm 2^\circ$ from the source earthquake. He found that earthquakes that are subject to a shear stress change of ≥ 0.01 MPa occurred up to 240 km from the source events. Huc and Main (2003) analyzed the global CMT data catalog ($M_w \geq 5.0$) and examined events that occurred within a time window of 30 days and a horizontal distance of 1500 km from the source events. They found no systematic triggering effect at a distance greater than the thickness of the Earth's lithosphere (100–150 km). Gasperini and Mulargia (1989) analyzed earthquakes with a magnitude $M \geq 4.0$ in and around Italy using the "influence region principle," which states that the lithospheric loads are modified by the occurrence of an earthquake within a certain time and distance from its origin. They found that triggering distances were in the range from 80 to 140 km. Their studies are not inconsistent with our results, as they are distributed almost in the same range as our estimation (Table 5).

Table 5 Triggering distances evaluated by previous studies

Magnitude	Lapsed time (days)	Triggering distances ranges (km)	Source
$M \geq 4.0$	14–60	80–140	Gasperini and Mulargia (1989)
$M \geq 7.0$	30–60	300–1000	Lomnitz (1996)
$M \geq 7.0$	> 0	~ 240	Parsons (2002)
$M \geq 5.0$	1–300	100–150	Huc and Main (2003)

Our results show an exponential decay of the triggering distance with lapsed time, and the characteristic time is about 400 days (Fig. 8b, d). This is not the same as the results of Huc and Main (2003) that showed that the triggering distance increases with time following a power-law growth characterized by t^H with $H = 0.05 - 0.06$, which results from a homogeneous diffusion process (e.g., Marsan et al. 2000). Such growth may be recognized, because aftershocks occurring close to the mainshock are included in their analyses. However, including or removing aftershocks close to the hypocenter of the mainshock may introduce some differences in temporal changes of the triggering distance, which suggests a different triggering mechanism.

On the other hand, several studies use the linear seismic density method to understand the triggering process of mainshock (Felzer and Brodsky 2006; Richards-Dinger et al. 2010). We apply the linear density method to the successive earthquakes we define instead of using all earthquakes. Following the computation procedure as shown in Additional file 1: Figure S1b of Richards-Dinger et al. (2010), we stack all the source events of clusters determined in "Results" section and sort all their dependent events by distance from their source event. We calculate the interval distance between nearby dependent

events (we term that distance "midpoints", the distance of two nearby midpoints is termed the width (W_i)). We calculate the linear seismic density for each width as the reciprocal of W_i ($1/W_i$). We then plot the obtained linear seismic density as a function of distance. Previous studies indicate that the linear seismicity density gradually decreases with distance from mainshocks and fluctuates at a background level at far distances. The distance where the slope of linear seismicity density changes represents the limit range of triggering by mainshocks. Additional file 1: Figures S8 and S9 plot the linear seismicity density of dependent earthquakes versus the distance from the source events for global CMT and F-net catalogs, respectively. The triggering distances we estimated in "Analysis of global CMT catalog" and "Analysis of NIED F-net catalog" sections are also indicated. For the global CMT catalog, the linear seismicity densities at small magnitude ranges of $M_w \leq 6.5$ show some trend changes at the distances less or around the triggering distances we estimated. Such trends are significant for short lapse times of 60 days but diminish with increasing lapse time. Contrary, the linear seismicity density in a large magnitude range is scattered and sparse so that no systematic feature is recognized. The linear seismicity density for the F-net catalog is also scattered and no significant trend is recognized even for small magnitude ranges. This is probably because the small numbers of data are not enough to show up a trend change in the plots which are the cases of a large magnitude range of global CMT catalog and all of F-net catalog. Alternatively, our method may determine the triggering distances for such a small-sized data set.

Conclusions

We have developed a method to systematically detect successive earthquakes for a wide magnitude range and applied the method to recent reliable global and regional catalogs. The detected successive earthquakes are compared with those obtained from simulated data in which the earthquakes are assumed to randomly occur over time to evaluate the triggering distance, which defines the distance range, where successive earthquakes occur. We obtained the following main results:

1. The number of clusters of successive earthquakes for real data is always larger than the number for simulated data at shorter distances, and becomes similar to that for simulated data at long distances. This suggests that large earthquakes trigger nearby large earthquakes beyond the so-called aftershock areas. The triggering distances are, for example, estimated to be 65 km for $4.0 \leq M_w < 4.5$ and 600 km for $M_w \geq 7.0$ at a lapsed time of 60 days after the occurrence of the source event. These triggering distances are stably estimated without significant effects of the removal of aftershocks. Analyses of different regions using global and regional catalogs indicate that the triggering distances slightly change in different tectonic settings.
2. Analyses of global catalog data showed that successive earthquakes are distributed along all types of plate boundaries, such as subduction, transform, and divergence boundaries. The percentage of the number of successive earthquakes with respect to the total number of earthquakes in each region ranges from approximately 8% to 20% for earthquakes with $M_w \geq 5.5$. For small and moderate earthquakes that occurred in and around the Japanese islands from 2001 to 2010, which are summarized in the NIED F-net catalog, successive earthquakes account for approximately 3% to 14% of earthquakes with a magnitude $4.0 \leq M_w < 5.5$.
3. The triggering distance increases, being proportional to about 1/5 to 1/4 power of the seismic moment of the source event for a wide magnitude range of $M_w \geq 4.0$. The triggering distance exponentially decreases with time.
4. We analyzed pseudo data catalogs that conform to the ETAS model and found that the triggering distances are well matched with the results obtained from the real data catalogs. We further derived scaling relations between the triggering distance and seismic moment using ETAS parameters. The predicted relations are well matched with the observed exponent of 1/5 to 1/4. These consistencies strongly suggest that the estimation of ETAS parameters enables us to evaluate the occurrence possibility of successive earthquakes. Especially for large earthquakes, such evaluation may be useful for estimating seismic hazards.
5. Static stress changes in the surrounding medium introduced by a source event may partially play a role in generating successive earthquakes, because more than a half of the successive earthquakes occur at regions with positive ΔCFF.

Appendix

A1. Stability of the simulated data

We performed the simulations 100 times and obtained average numbers of clusters against the horizontal distance to estimate the triggering distance. The triggering distance is stabilized by taking an average from many simulations. In the present study, to evaluate the

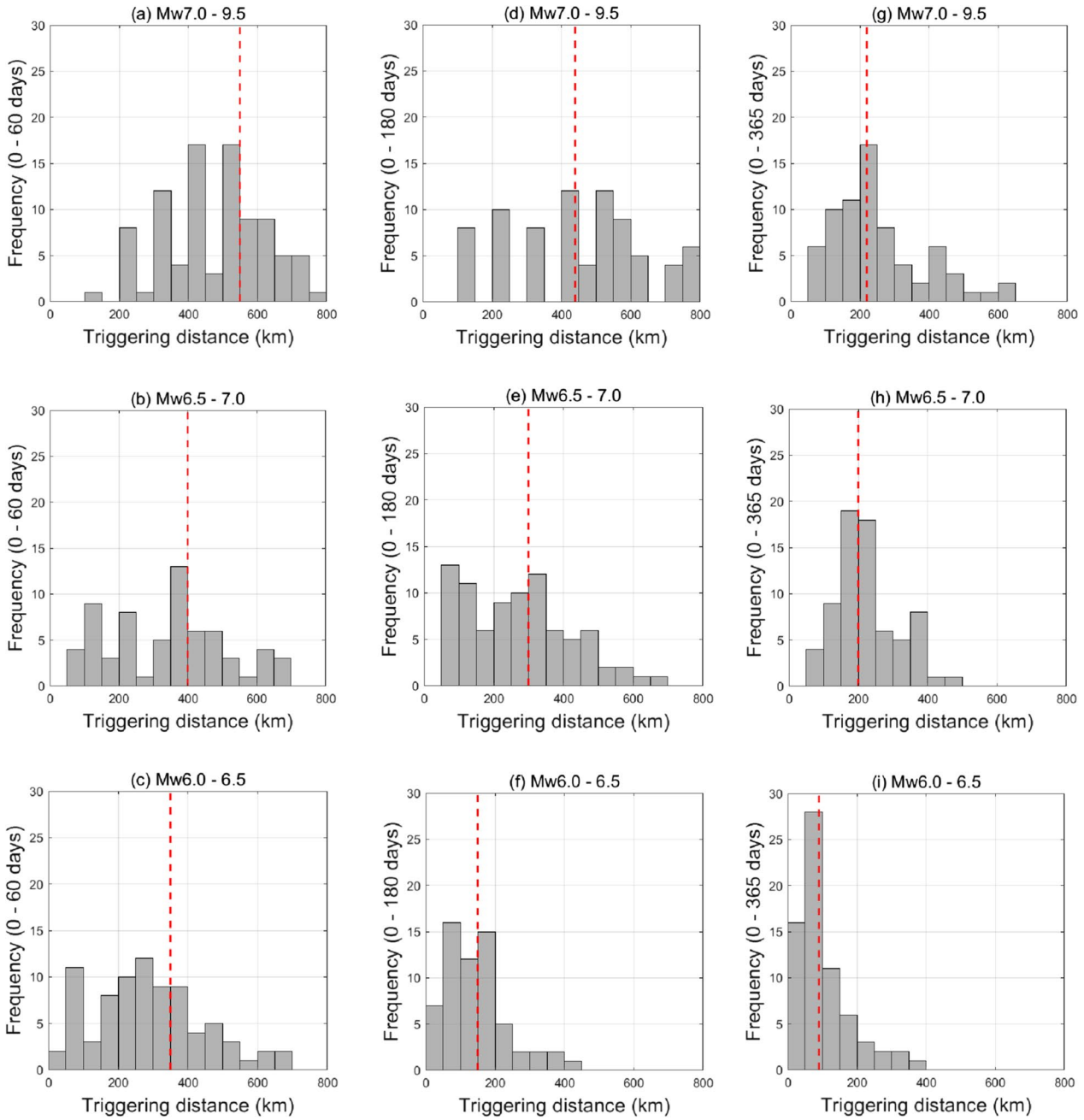

Fig. 11 Frequency distributions of the triggering distances calculated for 100 simulations. The observed triggering distances measured from the average of the 100 simulations are indicated by red dotted lines. Panels (**a**–**c**) represent frequency for lapsed time (T_a) of 60 days, **d**–**f** those for 180 days, and **g**–**i** those for 365 days

reliability of the solutions, we estimated the fluctuation of the triggering distance by comparing the number of clusters for real data to those for each simulated catalog. Figure 11 shows the frequencies of triggering distance obtained from 100 simulated catalogs for $T_a = 60$, 180, and 365 days and $t_d = 730$ days. The triggering distances are scattered over a few hundred kilometers, although the peaks of the frequencies almost match the triggering distances obtained from the averages of 100 simulations. As the magnitude range decreases or the lapsed time increases, the scatter seems to become smaller. This suggests that a large amount of data may reduce the

scatter and improve the reliability. We then calculated the standard deviations for the 100 sets and report the results within the plots of the triggering distance as error bars.

A2. Effects of parameters used for removing aftershocks

Parameters t_d and c play a key role in the selection of the source events that are used as the first source event in each cluster and consequently for the selection of dependent earthquakes. For example, using smaller c introduces a small area of aftershocks, meaning that more earthquakes become candidates for successive earthquakes, which may change the number of clusters, especially in a small horizontal distance range. Hence, the judicious choice of these two parameters must surely help to avoid an overestimation or underestimation of the triggering distance. However, there is no substantial rule for setting these parameters, so that ambiguity remains in their selections. In this subsection of the appendix, therefore, we examine how these two parameters affect the detection of successive earthquakes and estimation of the triggering distances.

Aftershocks are considered to occur within a region limited to 2–3 times the dimensions of the mainshock dimensions, and this region expands somewhat with time (days or years) (Utsu et al. 1995). The duration of an aftershock sequence (t_d) represents the time interval from the mainshock, where seismic activity goes back to the average daily background rate r (Utsu et al. 1995). The duration of aftershock sequences for a given mainshock has been discussed (e.g., Dieterich 1994; Marsan and Lengline 2008), but it is still subject to debate, because there is no standard or comprehensible criterion to efficiently define t_d. The duration of aftershock sequences is examined for tectonic settings, plate boundary type, and the faulting style of the mainshock (Tahir and Grasso 2013; Valerio et al. 2017; Toda and Stein 2018). In the present study, we calculated the values of t_d for the following seismic sequences: the 1992 M_w 7.3 earthquake in California, the 1993 M_w 7.8 and the 1994 M_w 7.7 earthquakes in Japan, the 1999 M_w 7.4 earthquake in Turkey, and the 2010 M_w 7.2 earthquake in New Zealand. We determined 2 years of background rate r (Utsu et al. 1995; Tahir and Grasso 2013) and estimated the modified Omori law decay parameters with fitting equation $R(t) = K/(t + c)^p$ for the [10 years, $D_{\min}$] window using a bootstrap method (Wiemer 2001; Sullivan and Peng 2012), where R is the number of events; t the elapsed time; and K, c, and p are constants. Figure 12 shows an example of the aftershock decay rate over time, and Table 6 summarizes the results for all values of $M_{\min}$. For earthquakes with $M \geq 5.0$ we set t_d to 730 days and tested the results for 365days and 180days. For small earthquakes with $M \leq 5.0$, we set t_d to 1825 days and tested the results for 730days and 365days. For the cases of (a) Landers and (d) Izmit earthquakes, the aftershock rates fall below the background rates. This is probably because the estimated background rate changes with time.

Fixing $c = 3$, we examined the effect of t_d on the detection of successive earthquakes. We found that the number of clusters mostly increased constantly with increasing lapsed time T_a and with increasing horizontal distance in a similar way for different t_d. Figure 13 shows the triggering distances for different aftershock durations. Differences among the estimated triggering distances for different aftershock durations are less than 17%, and no systematic change is recognized.

Fixing $t_d = 730$ days and $t_d = 1825$ days for the global CMT and NIED F-net catalogs, respectively, we examined the effect of the coefficient c on the detection of successive earthquakes. We found that decreasing c slightly increases the numbers of clusters at short distances. In contrast, the triggering distances for $c=2$ or $c=1$ are almost the same as those for $c=3$ (Fig. 14). These results suggest that the estimation of the triggering distance is not greatly affected by the selection of c.

In addition, we performed the same analysis when no aftershocks activities are removed from the catalog ($c = 0$). The results are shown in Additional file 1: Figure S3. The results are similar to the cases of $c=1$ to $c=3$. The triggering distance increases with the seismic moment and decreases with lapse time, although the estimated triggering distance seems to be smaller than the cases of $c=1$ to $c=3$. The reason is not known now, but may be due to some difference in the triggering process at near and far-fields or a limited number of data sets.

(See figure on next page.)

Fig. 12 Decays of aftershock rate over time for five mainshocks: **a** 1992 M_w 7.3 Landers earthquake, **b** 1993 M_w 7.8 Hokkaido–Nansei–Oki earthquake, **c** 1994 M_w 7.7 Sanriku–Oki earthquake, **d** 1999 M_w 7.4 Izmit earthquake, and **e** 2010 M_w 7.2 Darfield earthquake. The solid black line represents the aftershock decay predicted from the modified Omori law. The horizontal dashed red line represents the background seismicity rate for 2 years before the main shock. The vertical dashed blue lines are the estimated durations of the aftershock sequence, where the aftershock rate first goes to the average daily background rate (red dashed line). The parameters representing the modified Omori law parameters (p, c, and k) are indicated in each panel

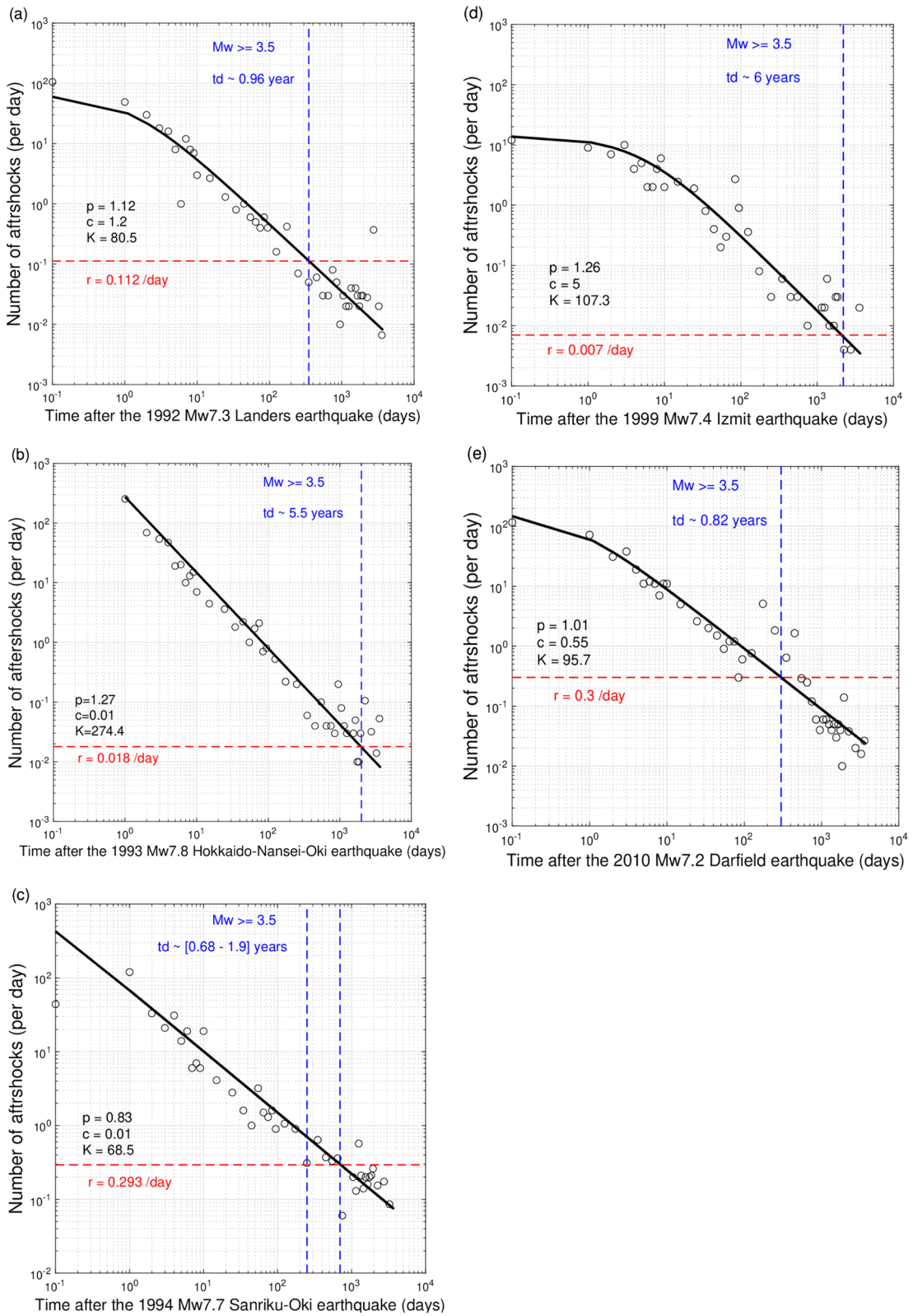

Fig. 12 (See legend on previous page.)

Table 6 Estimated aftershock durations

Mainshock	M_{min}	2-year Background (per day)	*k* value	*p* value	*c* value	t_d (year)
1992 M_w 7.3 Landers Eq	3.5	0.112	80.5	1.12	1.2	~0.96
	4.0	0.032	15	0.98	0.9	~1.5
	5.0	0.0014	12	1.04	5	~16.4
1993 M_w 7.8 Hokkaido–Nansei–Oki Eq	3.5	0.018	274.4	1.27	0.01	~5.5
	4.0	0.004	80.7	1.32	0.01	~4.9
	5.0	0.001	10	1.283	0.226	~3.6
1994 M_w 7.7 Sanriku–Oki Eq	3.5	0.293	68.5	0.83	0.01	~1.9
	4.0	0.138	38.7	0.89	0.01	~1.5
	5.0	0.022	10	0.99	0.01	~1.2
1999 M_w 7.4 Izmit Eq	3.5	0.007	107.3	1.26	5	~6
	4.5	0.007	17.9	1.13	0.01	~2.7
	5.0	0.007	12	1.18	5	~1.5
2010 M_w 7.2 Darfield Eq	3.5	0.3	95.7	1.01	0.55	~3.5
	4.0	0.3	17	0.95	0.01	~0.2
	5.0	0.3	10	0.82	5	~0.12

A3. Coulomb stress change on nodal planes

The change ΔCFF is expressed by $\Delta CFF = \Delta\tau + \mu'\Delta\sigma$, where $\Delta\tau$ and $\Delta\sigma$ are the shear and normal stress changes acting on the fault, respectively, and μ' is the apparent coefficient of friction (e.g., Reasenberg and Simpson 1992). We calculated ΔCFF for two nodal planes for a dependent event using a moment tensor solution of its source event. We calculated ΔCFF using the Coulomb3.3 program provided by the USGS (https://www.usgs.gov/software/coulomb-3). Because the global CMT catalog only provides a moment tensor solution, we assumed an appropriate fault length (in km) L and width W of a source event using an empirical relation for the magnitude and fault size presented in Wells and Coppersmith (1994): $L = 10^{-3.22+0.69M_w}$ and $W = 10^{-1.01+0.32M_w}$. We performed all calculations in an elastic half-space with a shear modulus 3.2×10^4 MPa and a Poisson's ratio of 0.25. The ΔCFF was calculated for two fault planes for all dependent events belonging to each cluster of successive earthquakes.

The Coulomb stress change is not the same for the two fault plane candidates predicted from a moment tensor solution. We may use one of the nodal planes, but this approach is only applicable to thoroughly investigated seismic events (Ishibe et al. 2017). Another approach is to use optimally oriented receiver faults, but we are not able to use it, because regional stress fields are not well investigated in all the regions of dependent earthquakes we determined. An alternative method is to compute ΔCFF for the two nodal planes predicted from the moment tensor solution. To deal with the issue, we calculated ΔCFF for both nodal planes and selected the one with the largest value. This has proven to be reliable for reducing the uncertainty of receiver faults in heterogeneous stress fields (i.e., Hardebeck et al. 1998; Nandan et al. 2016; Ishibe et al. 2017).

The computation of ΔCFF also depends on parameters, such as the friction and Skempton's coefficients, and it is often recommended to consider uncertainties associated with those parameters. However, numerical studies have indicated that realistic uncertainty estimates for the friction and Skempton's coefficients are modest in earthquake triggering (e.g., Harris 1998; Catalli et al. 2008; Nalbant et al. 2013; Wang et al. 2014). Here, we adopted an empirically introduced coefficient of friction of 0.4, because many previous studies show that this yields a strong correlation between earthquake occurrence and ΔCFF (e.g., Pollitz et al. 2003; Toda et al. 2011a; Toda and Stein 2013; Nalbant et al. 2013; Ishibe et al. 2017). Laboratory rock experiments indicate a higher friction coefficient, ranging between 0.5 and 0.8 (e.g., Byerlee and Brace 1968), but it is suggested that the coefficient of friction decreases when fluid is injected and pore-fluid pressure is increased (Skempton 1954). In the following analyses, we also analyzed the data using two other values ($\mu' = 0.2$ and $\mu' = 0.6$) for comparison. An example of the results for different coefficients of friction is given in Fig. 15.

The minimum Coulomb stress change that can trigger earthquakes is under discussion. Many previous studies suggest that static stress changes as low as 0.01 MPa (0.1 bar) can trigger aftershocks (e.g., Reasenberg and Simpson 1992; King et al. 1994; Hardebeck et al. 1998; Harris 1998; Toda et al. 1998). Because 0.01 MPa is just a fraction of the stress drop associated with the rupture

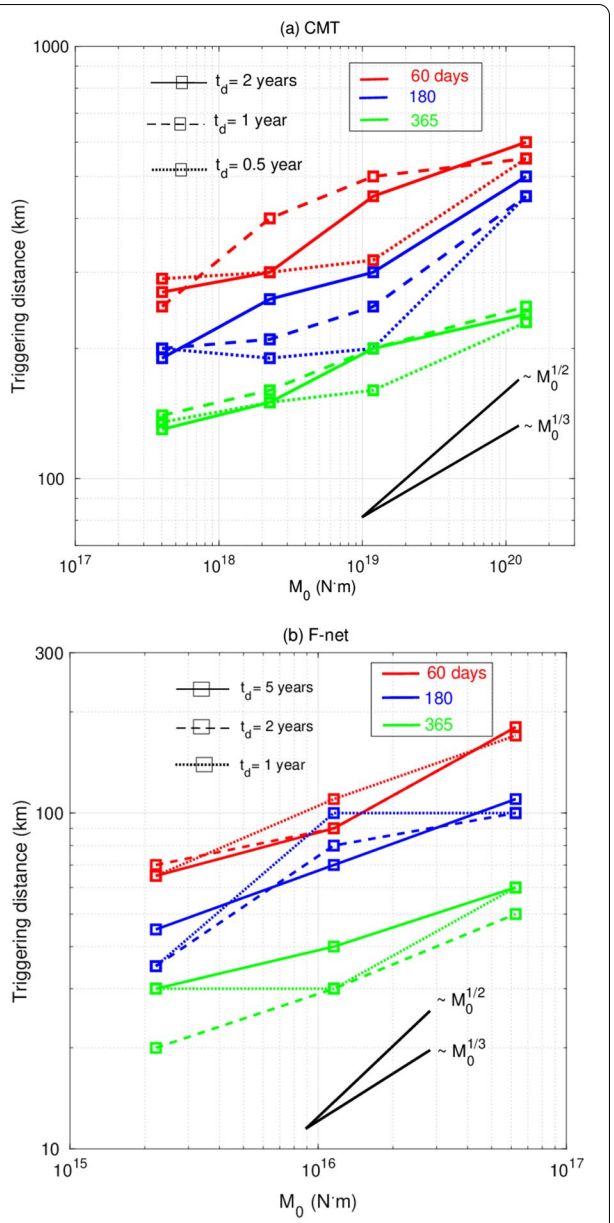

Fig. 13 Comparison of the triggering distances and seismic moment (M_0) estimated for different aftershock durations (t_d). **a** Results obtained from analyses of the global CMT catalog, where $t_d = 2$, 1, and 0.5 years are used. **b** Results obtained from analyses of the NIED F-net catalog, where $t_d = 5$, 2, and 1 years are used

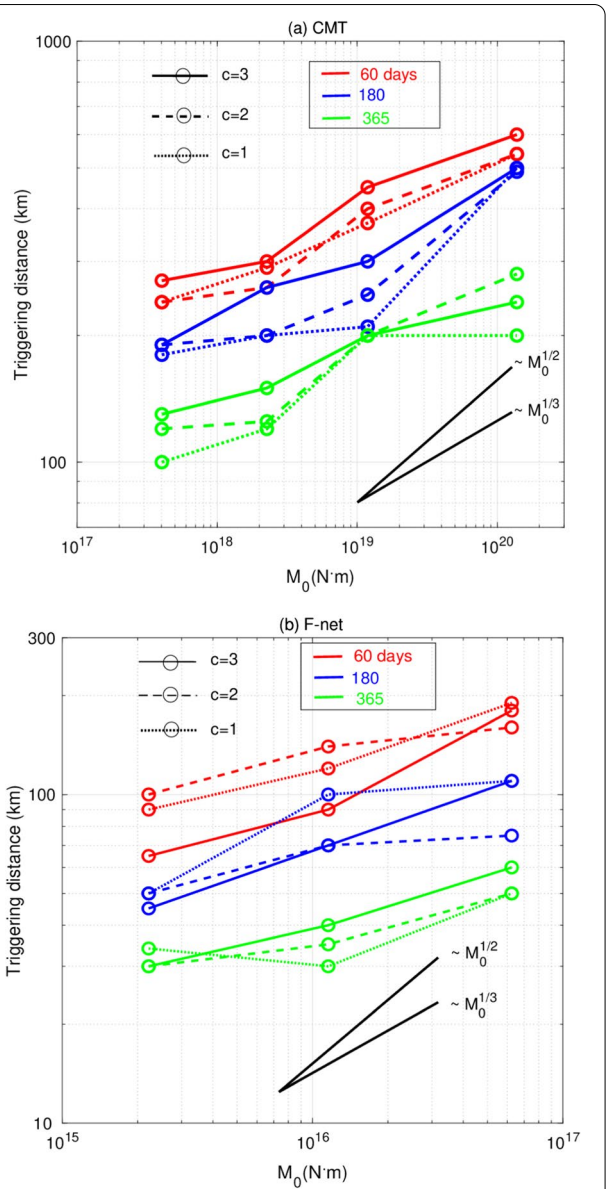

Fig. 14 Comparison of the triggering distances and seismic moment (M_0) estimated for different c values. **a** Results obtained from analyses of the global CMT catalog. **b** Results obtained from analyses of the NIED F-net catalog. $c = 3$, 2, and 1 are used

process of seismic faults, Harris (1998) suggested that the word "enhance" or "encourage" may better describe the triggering of an earthquake by ΔCFF than the word "generate." Although it may not be known whether a ΔCFF of 0.01 MPa sufficiently enhances or triggers earthquakes, several studies have indicated that the solid Earth tide (about 0.01 MPa) can trigger earthquakes (e.g., Tanaka et al. 2002a, b). In addition, Nandan et al. (2016) found strong evidence that a static stress of about 10 Pa is able to enhance seismicity, by analyzing earthquakes of magnitude $M \geq 2.5$ in Southern California. Positively stressed ($\Delta CFF > 0$) regions may generate more earthquakes than negatively stressed ($\Delta CFF < 0$) regions (Harris 1998; Toda et al. 2011a, b; Ishibe et al. 2017). In the present study, therefore, we examined two stress thresholds: 0 Pa and 10^3 Pa.

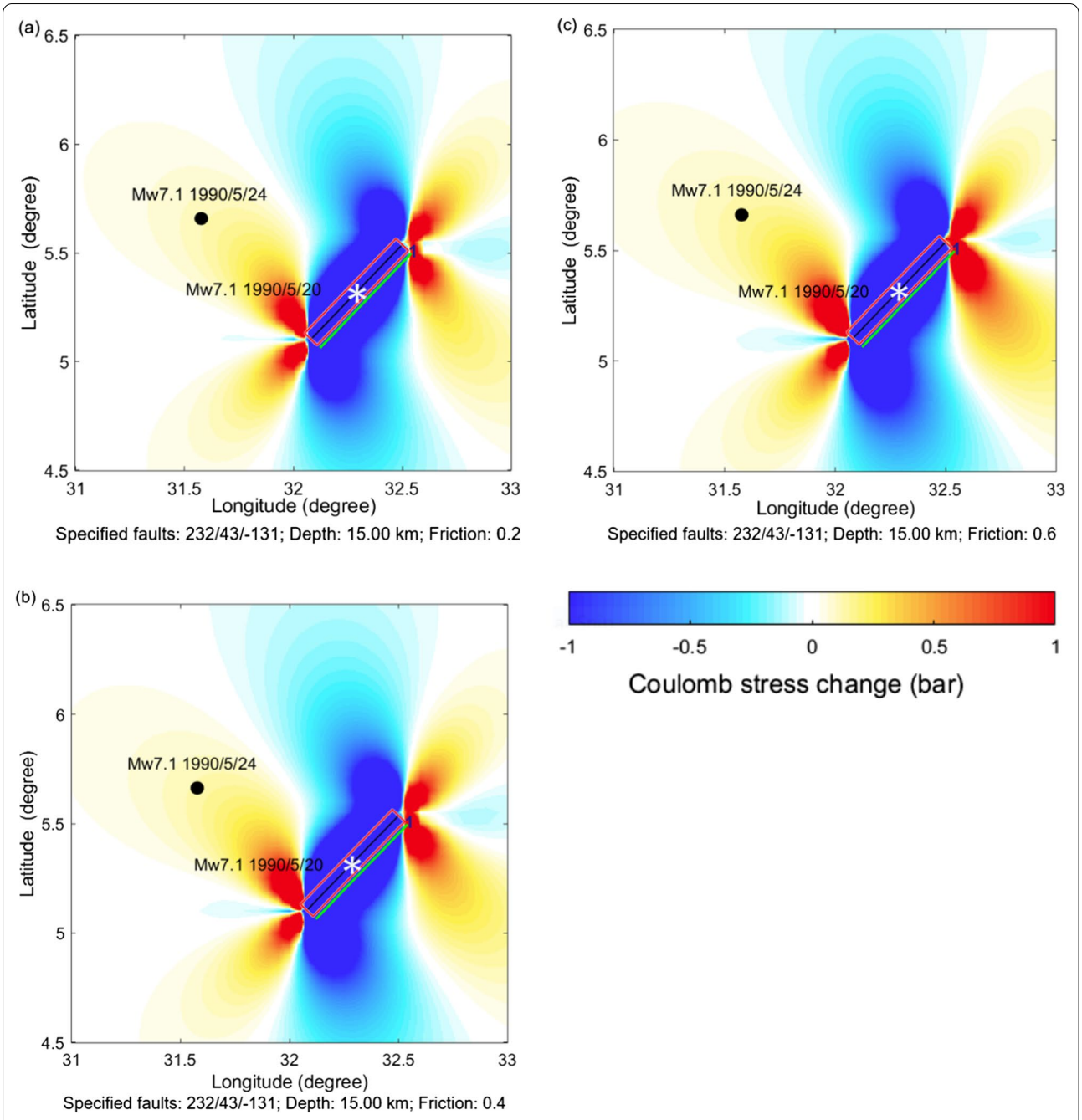

Fig. 15 Example of Δ*CFF* distributions caused by co-seismic slip of a source event. ΔCFF is calculated at a depth of 15 km for the plane that matches with one of the nodal planes of a dependent event. The coefficient of friction is **a** $\mu' = 0.2$, **b** $\mu' = 0.4$, and **c** $\mu' = 0.6$. Red indicates a positive ΔCFF that promotes failure, while blue indicates negative ones. The white asterisks indicate the centroid of the source event whose magnitude and occurrence date are shown together. The red rectangles represent the fault plane for the source event and the green lines represent the traces of the seismic fault on the ground surface. Black dots represent the locations of dependent events with their magnitude and occurrence date

Abbreviations
CMT: Centroid moment tensor; ETAS: Epidemic type aftershock sequence; NIED: National Research Institute for Earth Science and Disaster Prevention; ΔCFF: Coulomb failure function.

Supplementary Information

The online version contains supplementary material available at https://doi.org/10.1186/s40623-022-01677-4.

Additional file 1: Figure S1. Relation between the triggering distances and seismic moment (M_0) by counting the number clusters and the number of earthquakes. **a** Results obtained from analyses of global CMT and (**b**) results obtained from the analyses of NIED F-net catalogs. Solid and dashed lines represent clusters count and events count, respectively. **Figure S2.** Relation between the triggering distances and seismic moment (M_0) when the magnitude window is set fixed and variable. **a** Results obtained from analyses of global CMT and (**b**) results obtained from the analyses of NIED F-net catalogs. Solid and dashed lines represent fixed and variable magnitude windows, respectively. **Figure S3.** Relation between the triggering distances and seismic moment (M_0) by setting $c=3$ and $c=0$. (a) The results obtained from analyses of global CMT and, (b) the results obtained from the analyses of NIED F-net catalogs. Solid and dashed lines represent $c=3$ and $c=0$, respectively. **Figure S4.** Centroid distributions of (a) NIED F-net catalog and (b) an example of the synthetic ETAS catalog. Red dots are earthquakes with magnitude $3.5 \leq M_w \leq 5.5$ for the period from 1997 to 2010. **Figure S5.** Number of clusters versus horizontal distance for three lapsed times. Solid lines represent the results obtained from analyses of ETAS data and dotted lines those from simulated data catalogs. **a**–**k** Different ETAS catalogs for M_w 5.0–5.5, $c=3$, and $t_d=1825$ days. Arrows indicate the triggering distances (see the text). **Figure S6.** Number of clusters versus horizontal distance for three lapsed times. Solid lines represent the results obtained from analyses of ETAS data and dotted lines those from simulated data catalogs. **a**–**k** Different ETAS catalogs for M_w 4.5–5.0, $c=3$, and $t_d=1825$ days. Arrows indicate the triggering distances (see the text). Note that the ranges of the vertical axes are different for (a)–(f). **Figure S7.** Number of clusters versus horizontal distance for three lapsed times. Solid lines represent the results obtained from analyses of ETAS data and dotted lines those from simulated data catalogs. **a**–**k** Different ETAS catalogs for M_w 4.0–4.5, $c=3$, and $t_d=1825$ days. Arrows indicate the triggering distances (see text). Note that the ranges of the vertical axes are different for (**a**)–(**k**). **Figure S8.** Linear density of dependent events versus distance from the source event for global CMT. The blue line shows the triggering distances obtained in this study for global CMT catalog (see "Analysis of global CMT catalog" section). **Figure S9.** Linear density of dependent events versus distance from the source event for F-net. The blue line shows the triggering distances obtained in this study for F-net (see "Analysis of NIED F-net catalog" section).

Acknowledgements
We thank the associate editor Dr. Hideo Aochi and two anonymous reviewers for their comments on the original manuscript. We also thank Professor Shinji Toda (Tohoku University) for his suggestions, which improved the manuscript. We used CMT solutions provided by Colombia University, and the NIED F-net catalog is provided by NIED.

Author contributions
TMB performed data analyses with TN. Both authors discussed the results and contributed to the paper writing. Both authors read and approved the final manuscript.

Funding
TMB was supported by a scholarship program of the Ministry of Education, Culture, Sports, Science and Technology of Japan.

Availability of data and materials
We used the source parameters for earthquakes in the global CMT catalog (www.globalcmt.org) and NIED F-net catalog (https://www.fnet.bosai.go.jp/event/search.php?LANG=en). We used the following hypocenters to analyze the duration of the aftershock sequences: Southern California Earthquake Data Center, USA (https://scedc.caltech.edu/) for the 1992 M_w 7.3 Landers earthquake; JMA (http://www.data.jma.go.jp/svd/eqev/data/bulletin/index_e.html) for the 1993 M_w 7.8 Hokkaido–Nansei–Oki earthquake and the 1994 M_w 7.7 Sanriku–Oki earthquake; Kandilli Observatory and Earthquake Research Institute, Turkey (http://www.koeri.boun.edu.tr) for the 1999 M_w 7.6 Izmit earthquake; and the GeoNet, New Zealand (https://www.geonet.org.nz/) for the 2010 M_w 7.0 Darfield earthquake. MATLAB software packages Coulomb3.3 (https://www.usgs.gov/software/coulomb-3), ZMAP 7 (http://www.seismo.ethz.ch/en/research-and-teaching/products-software/software/ZMAP/), RunAftSimulator.m (https://web.archive.org/web/20200712004939/https://pasadena.wr.usgs.gov/office/kfelzer/AftSimulator.html) and m_map (Pawlowicz 2020) (https://www.eoas.ubc.ca/~rich/map.html) were used to calculate the Coulomb stress change, to analyze seismicity, to simulate the ETAS catalog, and to produce maps, respectively.

Declarations

Competing interests
The authors declare that they have no competing interests.

Received: 21 September 2021 Accepted: 15 July 2022
Published online: 27 July 2022

References

Arnadottir T, Geirsson H, Einarsson P (2004) Coseismic stress changes and crustal deformation on the Reykjanes Peninsula due to triggered earthquakes on 17 June 2000. J Geophys Res 109:B09307. https://doi.org/10.1029/2004JB003130
Bak P, Christensen K, Danon L, Scanlon T (2002) Unified scaling law for earthquakes. Phys Rev Lett 88(17):178501
Barka A (1996) Slip distribution along the North Anatolian fault associated with the large earthquakes of the period 1939 to 1967. Bull Seismol Soc Am 86(5):1238–1254
Båth M (1965) Lateral inhomogeneities in the upper mantle. Tectonophysics 2:483–514
Bird P, Kagan YY, Jackson DD, Stein S, Freymueller JT (2002) Plate tectonics and earthquake potential of spreading ridges and oceanic transform faults. In: Stein S, Freymueller JT (eds) Plate boundary zones, geodynamics series, 30. Am. Geophys. Union, Washington, DC, pp 203–218
Bormann P, Giacomo D (2010) The moment magnitude and the energy magnitude: common roots and differences. J Seismol 15:411–427. https://doi.org/10.1007/s10950-010-9219-2
Byerlee JD, Brace WF (1968) Stick-slip stable sliding and earthquakes-effect of rock type, pressure, strain rate, and stiffness. J Geophys Res 73(18):6031–6037
Catalli F, Cocco M, Console R, Chiaraluce L (2008) Modeling seismicity rate changes during the 1997 Umbria-Marche sequence (central Italy) through a rate- and state-dependent model. J Geophys Res 113:B11301. https://doi.org/10.1029/2007JB005356
Chiba K (2022) Heterogeneous b-value distributions measured over an extensive region from the Northern Okinawa Trough to Southern Kyushu Island Japan. Pure Appl Geophys 179(3):899–913
Chu A, Schoenberg FP, Bird P, Jackson DD, Kagan YY (2011) Comparison of ETAS parameter estimates across different global tectonic zones. Bull Seismol Soc Am 101(5):2323–2339. https://doi.org/10.1785/0120100115
Console R, Murru M, Catalli F, Falcone G (2007) Real time forecasts through an earthquake clustering model constrained by the rate-and-state constitutive law: comparison with a purely stochastic ETAS model. Seismol Res Lett 78(1):49–56
Corral Á (2004a) Long-term clustering, scaling, and universality in the temporal occurrence of earthquakes. Phys Rev Lett 92(10):108501. https://doi.org/10.1103/PhysRevLett.92.108501
Corral Á (2004b) Universal local versus unified global scaling laws in the statistics of seismicity. Physica A 340(4):590–597. https://doi.org/10.1016/j.physa.2004.05.010

Corral Á (2008) Scaling and universality in the dynamics of seismic occurrence and beyond. In: Carpinteri A, Lacidogna G (eds) Acoustic emission and critical phenomena. Taylor & Francis Group, London, pp 225–244. https://doi.org/10.1201/9780203892220.ch2.2

Daley DJ, Vere-Jones D (2003) An introduction to the theory of point processes, Vol I, 2nd edn. Springer, Berlin

Dascher-Cousineau K, Brodsky EE, Lay T, Goebel T (2020) What controls variations in aftershock productivity? J Geophys Res 125:e2019JB018111. https://doi.org/10.1029/2019JB018111

Davidsen J, Paczuski M (2005) Analysis of the spatial distribution between successive earthquakes. Phys Rev Lett 94(4):048501. https://doi.org/10.1103/PhysRevLett.94.048501

de Arcangelis L, Lippiello E, Godano C, Nicodemi M (2008) Statistical properties and universality in earthquake and solar flare occurrence. Eur Phys J B 64:551–555. https://doi.org/10.1140/epjb/e2008-00057-5

Dieterich J (1994) A constitutive law for rate of earthquake production and its application to earthquake clustering. J Geophys Res 99:2601–2618

Dziewonski AM, Chou TA, Woodhouse JH (1981) Determination of earthquake source parameters from waveform data for studies of global and regional seismicity. J Geophys Res 86:2825–2852. https://doi.org/10.1029/JB086iB04p02825

Earthquake Research Committee (2020) Seismic Activity in Japan -Regional perspectives on the characteristics of destructive earthquakes. https://www.hp1039.jishin.go.jp/eqchreng/eqchrfrm.htm.

Ekström G, Nettles M, Dziewonski AM (2012) The global CMT project 2004–2010: Centroid-moment tensors for 13,017 earthquakes. Phys Earth Planet Int 200:1–9. https://doi.org/10.1016/j.pepi.2012.04.002

Enescu B, Ito K (2003) Values of b and p: their variations and relation to physical processes for earthquakes in Japan. Ann Disaster Prev Res Inst Kyoto Univ 46:709–719

Felzer KR, Brodsky EE (2006) Decay of aftershock density with distance indicates triggering by dynamic stress. Nature 441:735–738. https://doi.org/10.1038/nature04799

Felzer KR, Becker TW, Abercrombie RE, Ekström G, Rice RG (2002) Triggering of the 1999 Mw 7.1 Hector Mine earthquake by aftershocks of the 1992 Mw 7.3 Landers earthquake. J Geophys Res 107:2190. https://doi.org/10.1029/2001JB000911

Freed MA (2005) Earthquake triggering by static, dynamic, and postseismic stress transfer. Annu Rev Earth Planet Sci 33:335–367. https://doi.org/10.1146/annurev.earth.33.092203.122505

Freed AM, Lin J (2001) Delayed triggering of the 1999 Hector Mine earthquake by viscoelastic stress transfer. Nature 411:180–183

Gardner JK, Knopoff L (1974) Is the sequence of earthquakes in southern California, with aftershocks removed, Poissonian? Bull Seismol Soc Am 64:1363–1367

Gasperini P, Mulargia F (1989) A statistical analysis of seismicity in Italy: the clustering properties. Bull Seismol Soc Am 79:973–988

Goda K, Campbell G, Hulme L, Ismael B, Ke L, Marsh R, Sammonds P, So E, Okumura Y, Kishi N, Yotsui S, Kiyono J, Wu S, Wilkinson S (2016) The 2016 Kumamoto earthquakes: cascading geological hazards and compounding risks. Front Built Environ 2:19. https://doi.org/10.3389/fbuil.2016.00019

Gomberg J, Johnson P (2005) Dynamic triggering of earthquakes. Nature 437(7060):830. https://doi.org/10.1038/437830a

Guo Y, Zhuang J, Zhou S (2015) An improved space-time ETAS model for inverting the rupture geometry from seismicity triggering. J Geophys Res 120:3309–3323. https://doi.org/10.1002/2015JB011979

Gutenberg B, Richter C (1944) Frequency of earthquakes in California. Bull Seismol Soc Am 34:185–188

Hanks C, Kanamori H (1979) A moment magnitude scale. J Geophys Res 84:2348–2350

Hardebeck JL, Nazareth JJ, Hauksson E (1998) The static stress change triggering model: Constraints from two southern California aftershock sequences. J Geophys Res 103(B10):24427–24437. https://doi.org/10.1029/98JB00573

Hardebeck JL, Felzer KR, Michael AJ (2008) Improved tests reveal that the accelerating moment release hypothesis is statistically insignificant. J Geophys Res 113:B08310. https://doi.org/10.1029/2007JB005410

Harris RA (1998) Introduction to special section: stress triggers, stress shadows, and implications for seismic hazard. J Geophys Res 103(B10):24347–24358. https://doi.org/10.1029/98JB01576

Helmstetter A, Sornette D (2004) Comment on "Power-law time distribution of large earthquakes." Phys Rev Lett. https://doi.org/10.1103/PhysRevLett.92.129801

Hickman S, Sibson R, Bruhn R (1995) Introduction to special section: mechanical involvement of fluids in faulting. J Geophys Res 100:12831–12840. https://doi.org/10.1029/95JB01121

Hicks A (2011) Clustering in multidimensional spaces with applications to statistical analysis of earthquake clustering, in M.Sc Thesis, Department of Mathematics and Statistics, University of Nevada, Reno, August, 2011

Hill DP, Reasenberg PA, Michael A, Arabaz WJ, Beroza G, Brumbaugh D, Brune JN, Castro R, Davis S, dePolo D, Ellsworth WL, Gomberg J, Harmsen S, House L, Jackson SM, Johnston MJS, Jones L, Keller R, Malone S, Munguia L, Nava S, Pechmann JC, Sanford A, Simpson RW, Smith RB, Stark M, Stickney M, Vidal A, Walter S, Wong V, Zollweg J (1993) Seismicity remotely triggered by the magnitude 7.3 Landers, California, earthquake. Science 260:1617–1623. https://doi.org/10.1126/science.260.5114.1617

Hill DP, Prejean SG (2006) Chap 8—Dynamic triggering. In: Schubert G (ed) Treatise on geophysics, Vol 4. Kanamori H (ed) "Earthquake seismology"

Huc M, Main IG (2003) Anomalous stress diffusion in earthquake triggering: correlation length, time dependence, and directionality. J Geophys Res 108(B7):2324. https://doi.org/10.1029/2001JB001645

Ishibe T, Ogata Y, Tsuruoka H, Satake K (2017) Testing the Coulomb stress triggering hypothesis for three recent megathrust earthquakes. Geosci Lett 4:5. https://doi.org/10.1186/s40562-017-0070-y

Iwata T (2013) Estimation of completeness magnitude considering daily variation in earthquake detection capability. Geophys J Int 194:1909–1919. https://doi.org/10.1093/gji/ggt208

Japan Meteorological Agency (2013) National Catalogue of the Active Volcanoes in Japan (4th edn, English version). Japan Meteorological Agency and Volcanological Society of Japan. https://www.data.jma.go.jp/svd/vois/data/tokyo/STOCK/souran_eng/menu.htm

Kagan YY, Knopoff L (1980) Spatial distribution of earthquakes: the two-point correlation function. Geophys J Int 62:303–320. https://doi.org/10.1111/j.1365-246X.1980.tb04857.x

Kanamori H, Anderson DL (1975) Theoretical basis of some empirical relationships in seismology. Bull Seismol Soc Am 65:1073–1095

King GCP, Stein RS, Lin J (1994) Static stress changes and triggering of earthquakes. Bull Seismol Soc Am 84(3):935–953

Kubo A, Fukuyama E, Kawai H, Nonomura K (2002) NIED seismic moment tensor catalogue for regional earthquakes around Japan: quality test and application. Tectonophysics 356(2002):23–48

Kumazawa T, Ogata Y (2014) Nonstationary ETAS models for nonstandard earthquakes. Ann Appl Stat 8(3):1825–1852. https://doi.org/10.1214/14-AOAS759

Lombardi AM (2016) Some reasoning on the improvement of the ETAS modeling at the occurrence of the 2016 Central Italy seismic sequence. Ann Geophys, 59, Fast track 5. https://doi.org/10.4401/ag-7202.

Lomnitz C (1996) Search of a worldwide catalog for earthquakes triggered at intermediate distances. Bull Seismol Soc Am 86:293–298

Marekova E (2014) Analysis of the spatial distribution between successive earthquakes occurred in various regions in the world. Acta Geophys. https://doi.org/10.2478/s11600-014-0234-5

Marsan D, Enescu B (2012) Modeling the foreshock sequence prior to the 2011, MW9.0 Tohoku, Japan, earthquake. J Geophys Res 117:B06316. https://doi.org/10.1029/2011JB009039

Marsan D, Lengline O (2008) Extending earthquakes' reach through cascading. Science 319(5866):1076–1079. https://doi.org/10.1126/science.1148783S

Marsan D, Lengline O (2010) A new estimation of the decay of aftershock density with distance to mainshock. J Geophys Res. https://doi.org/10.1029/2009JB007119

Marsan D, Bean CJ, Steacy S, McCloskey J (2000) Observations of diffusion processes in earthquake populations and implications for the predictability of seismicity systems. J Geophys Res 105:28081–28094

Marzocchi W, Lombardi AM (2008) A double branching model for earthquake occurrence. J Geophys Res 113(B08):317. https://doi.org/10.1029/2007JB005472

Michael AJ (2011) Random variability explains apparent global clustering of large earthquakes. Geophys Res Lett. https://doi.org/10.1029/2011GL049443

Mignan A, Woessner J (2012) Estimating the magnitude of completeness for earthquake catalogs. Community Online Resour Stat Seism Anal. https://doi.org/10.5078/corssa-00180805
Nakano M, Nakamura T, Kamiya S, Ohori M, Kaneda Y (2013) Intensive seismic activity around the Nankai trough revealed by DONET ocean-floor seismic observations. Earth Planets Space 65:5–15. https://doi.org/10.5047/eps.2012.05.013
Nakata T, Imaizumi T (2002) Digital active fault map of Japan. University of Tokyo Press, Tokyo
Nalbant S, McCloskey J, Steacy S, NicBhloscaidh M, Murphy S (2013) Interseismic coupling, stress evolution, and earthquake slip on the Sunda megathrust. Geophys Res Lett 40:4204–4208. https://doi.org/10.1002/grl.50776
Nandan S, Ouillon G, Woessner J, Sornette D, Wiemer S (2016) Systematic assessment of the static stress-triggering hypothesis using inter-earthquake time statistics. J Geophys Res 121:1890–1909. https://doi.org/10.1002/2015JB012212
Nanjo KZ, Yoshida A (2021) Changes in the b value in and around the focal areas of the M6.9 and M6.8 earthquakes off the coast of Miyagi prefecture, Japan, in 2021. Earth Planets Space 73(1):1–10. https://doi.org/10.1186/s40623-021-01511-3
Nanjo KZ, Ishibe T, Tsuruoka H, Schorlemmer D, Ishigaki Y, Hirata N (2010) Short note analysis of the completeness magnitude and seismic network coverage of Japan. Bull Seismol Soc Am. https://doi.org/10.1785/0120100077
Nishimura T (2017) Triggering of volcanic eruptions by large earthquakes. Geophys Res Lett 44:7750–7756. https://doi.org/10.1002/2017GL074579
Ogata Y (1988) Statistical models for earthquake occurrences and residual analysis for point processes. J Am Stat Assoc 83(401):9–27
Ogata Y (1998) Space–time point-process models for earthquake occurrences. Ann Inst Stat Math 50:379–402
Ogata Y (2004) Space-time model for regional seismicity and detection of crustal stress changes. J Geophys Res. https://doi.org/10.1029/2003JB002621
Ogata Y, Zhuang (2006) Space–time ETAS models and an improved extension. Tectonophysics 413:13–23
Ogata Y, Katsura K, Tanemura M (2003) Modelling heterogeneous space–time occurrences of earthquakes and its residual analysis. Appl Stat 4:499–509
Okada Y, Kasahara K, Hori S, Obara K, Sekiguchi S, Fujiwara H, Yamamoto A (2004) Recent progress of seismic observation networks in Japan—Hi-net, F-net, K-NET and KiK-net. Earth Planet Space 56:xv–xxviii. https://doi.org/10.1186/BF03353076
Omori F (1894) On the aftershocks of earthquakes. J Coll Sci Imperial Univ Tokyo 7:111–120
Parsons T (2002) Global Omori law decay of triggered earthquakes: large aftershocks outside the classical aftershock zone. J Geophys Res 107(B9):2199. https://doi.org/10.1029/2001JB000646
Pawlowicz R (2020) "M_Map: A mapping package for MATLAB", version 1.4m, Computer software. www.eoas.ubc.ca/~rich/map.html.
Pollitz F, Vergnolle M, Calais E (2003) Fault interaction and stress triggering of twentieth century earthquakes in Mongolia. J Geophys Res 108(B10):2503. https://doi.org/10.1029/2002JB002375
Prejean SG, Hill DP, Brodsky EE, Hough SE, Johnston MJS, Malone SD, Oppenheimer DH, Pitt AM, Richards-Dinger KB (2004) Remotely triggered seismicity on the United States west coast following the Mw 7.9 Denali fault earthquake. Bull Seismol Soc Am 94(6B):S348–S359
Reasenberg PA (1999) Foreshock occurrence before large earthquakes. J Geophys Res 104(B3):4755–4768
Reasenberg PA, Simpson RW (1992) Response of regional seismicity to the static stress change produced by the Loma Prieta earthquake. Science 255:1687–1690
Richards-Dinger K, Stein RS, Toda S (2010) Decay of aftershock density with distance does not indicate triggering by dynamic stress. Nature 467:583–586. https://doi.org/10.1038/nature09402
Seif S, Mignan A, Zechar JD, Werner MJ, Wiemer S (2017) Estimating ETAS: the effects of truncation, missing data, and model assumptions. J Geophys Res Solid Earth 122:449–469. https://doi.org/10.1002/2016JB012809
Sevilgen V, Stein RS, Pollitz FF (2012) Stress imparted by the great 2004 Sumatra earthquake shut down transforms and activated rifts up to 400 km away in the Andaman Sea. PNAS 109(38):15152–15156. https://doi.org/10.1073/pnas.1208799109
Shearer PM, Stark PB (2012) Global risk of big earthquakes has not recently increased. Proc Nat Acad Sci USA 109(3):717–721. https://doi.org/10.1073/pnas.1118525109
Sibson RH, Moore JMcM, Rankin AH (1975) Seismic pumping: a hydrothermal fluid transport mechanism. J Geol Soc Lond 131:652–659
Sibson RH (1981) Fluid flow accompanying faulting: field evidence and models, earthquake prediction. In: Simpson DW, Richards PG (ed) International review. Am Geophys Union, Maurice Ewing Series 4, pp 593–603
Skempton AW (1954) The pore pressure coefficients A and B. Geotechnique 4(4):143–147. https://doi.org/10.1680/geot.1954.4.4.143
Stein RS (1999) The role of stress transfer in earthquake occurrence. Nature 402(6762):605–609
Sullivan B, Peng Z (2012) Statistical Seismology Tutorial. www.geophysics.eas.gatech.edu/people/bsullivan/tutorial/StatisticalSeismology.htm.
Tahir M, Grasso JR (2013) Aftershock patterns of ms >7 earthquakes in the India-Asia collision belt: anomalous results from the Muzaffarabad earthquake sequence, Kashmir, 2005. Bull Seismol Soc Am 104(1):1–23
Taira A (2001) Tectonic evolution of the Japanese island arc system. Annu Rev Earth Planet Sci 29:109–134
Tanaka S, Ohtake M, Sato H (2002a) Spatio-temporal variation of the tidal triggering effect on earthquake occurrence associated with the 1982 South Tonga earthquake of Mw 7.5. Geophys Res Lett 29(16):1756. https://doi.org/10.1029/2002aGL015386
Tanaka S, Ohtake M, Sato H (2002b) Evidence for tidal triggering of earthquakes as revealed from statistical analysis of global data. J Geophys Res 107(B10):2211. https://doi.org/10.1029/2001JB001577
Tibi R, Wiens DA, Inoue H (2003) Remote triggering of deep earthquakes in the 2002 Tonga sequence. Nature 424:921–925
Toda S, Stein RS (2013) The 2011 M = 9.0 Tohoku oki earthquake more than doubled the probability of large shocks beneath Tokyo. Geophys Res Lett 40:2562–2566. https://doi.org/10.1002/grl.50524
Toda S, Stein RS (2018) Why aftershock duration matters for probabilistic seismic hazard assessment. Bull Seismol Soc Am 108(3A):1414–1426. https://doi.org/10.1785/0120170270.U.S
Toda S, Stein RS, Reasenberg PA, Dieterich JH, Yoshida A (1998) Stress transferred by the 1995 Mw= 6.9 Kobe, Japan, shock: effect on aftershocks and future earthquake probabilities. J Geophys Res: Solid Earth 103(B10):24543–24565
Toda S, Lin J, Meghraoui M, Stein RS (2008) 12 May 2008 M=7.9 Wenchuan, China, earthquake calculated to increase failure stress and seismicity rate on three major fault systems. Geophys Res Lett 35:L17305. https://doi.org/10.1029/2008GL034903
Toda S, Stein RS, Sevilgen V, Lin J (2011a) Coulomb 3.3 Graphic-rich deformation and stress-change software for earthquake, tectonic, and volcano research and teaching-user guide. U.S. Geological Survey. Open-File Report 2011a–1060. https://pubs.usgs.gov/of/2011a/1060/of2011a-1060.pdf. Accessed 21 Feb 2017.
Toda S, Lin J, Stein RS (2011b) Using the 2011 Mw 9.0 off the Pacific coast of Tohoku earthquake to test the Coulomb stress triggering hypothesis and to calculate faults brought closer to failure. Earth Planets Space 63:725–730. https://doi.org/10.5047/eps.2011.05.010
U.S. Geological Survey (2021) Three notable earthquakes struck in the southern Pacific Ocean near the Kermadec Islands and New Zealand today, March 4, 2021. https://www.usgs.gov/news/featured-story/kermadec-and-new-zealand-earthquakes
Utsu T (1955) A relation between the area of after-shock region and the energy of main-shock. J Seismol Soc Jpn 2(7):233–240
Utsu T (1957) Magnitude of earthquakes and occurrence of their aftershocks. J Seismol Soc Jpn 10:35–45 (**in Japanese with English abstract**)
Utsu T (2002) Statistical features of seismicity. In: Lee WHK (ed) International handbook of earthquake & engineering seismology part A. Academic, San Diego, pp 719–773
Utsu T, Ogata Y, Matsu'ura R (1995) The centenary of the Omori formula for a decay law of aftershocks activity. J Phys Earth 43(1):1–33. https://doi.org/10.4294/jpe1952.43.1
Valerio E, Tizzani P, Carminati E, Doglioni C (2017) Longer aftershocks duration in extensional tectonic settings. Sci Rep 7:16403. https://doi.org/10.1038/s41598-017-14550-2

van der Elst NJ, Brodsky EE (2010) Connecting near-field and far-field earthquake triggering to dynamic strain. J Geophys Res 115:B07311. https://doi.org/10.1029/2009JB006681
Van Stiphout TJ, Zhuang, Marsan D (2012) Seismicity declustering. Community Online Resour Stat Seism Anal. https://doi.org/10.5078/corssa-52382934
Wang J, Xu C, Freymueller JT, Li Z, Shen W (2014) Sensitivity of Coulomb stress change to the parameters of the Coulomb failure model: a case study using the 2008 Mw 7.9 Wenchuan earthquake. J Geophys Res 119:3371–3392. https://doi.org/10.1002/2012JB009860
Wells DL, Coppersmith KJ (1994) New empirical relationships among magnitude, rupture length, rupture width, rupture area, and surface displacement. Bull Seismol Soc Am 84(4):974–1002
Wiemer S (2001) A software package to analyze seismicity: ZMAP. Seism Res Lett 72(3):373–382. https://doi.org/10.1785/gssrl.72.3.373
Wiemer S, Wyss M (2000) Minimum magnitude of completeness in earthquake catalogs: examples from Alaska, the Western United States, and Japan. Bull Seismol Soc Am 90(4):859–869. https://doi.org/10.1785/0119990114
Zaliapin I, Ben-Zion Y (2016) A global classification and characterization of earthquake clusters. Geophys J Int 207:608–634. https://doi.org/10.1093/gji/ggw300
Zhuang J, Ogata Y, Vere-Jones D (2004) Analyzing earthquake clustering features by using stochastic reconstruction. J Geophys Res 109:B05301. https://doi.org/10.1029/2003JB002879
Zhuang J, Werner MJ, Hainzl S, Harte D, Zhou S (2011) Basic models of seismicity: spatiotemporal models. Comm Online Res Stat Seism Anal. https://doi.org/10.5078/corssa-07487583

Publisher's Note